JOURNAL OF GEOPHYSICAL RESEARCH, VOL. 104, NO. E11, PAGES 27,043-27,066, NOVEMBER 25, 1999

Effects of sterilizing doses of gamma radiation on Mars analog rocks and minerals

Carlton C. Allen,[1] Fred G. Albert,[2] Joan Combie,[2] Amos Banin,[3] Yehuda Yablekovitch,[3] Ido Kan,[3] Robert J. Bodnar,[4] Victoria E. Hamilton,[5] Bradley L. Jolliff,[6] Karla Kuebler,[6] Alian Wang,[6] David J. Lindstrom,[7] Penny A. Morris,[8] Richard V. Morris,[7] Richard W. Murray,[9] Laurence E. Nyquist,[7] Paul D. Simpson,[10] Andrew Steele,[11] and Steven J. Symes[7]

Abstract. Rock and soil samples from the planet Mars are due to be returned to Earth within a decade. Martian samples initially will be tested for evidence of life and biological hazard under strict biological containment. Wider distribution of samples for organic and inorganic analysis may occur only if neither evidence of life nor hazard is detected, or if the samples are first sterilized. We subjected a range of Mars analog rocks and minerals to high doses of gamma radiation in order to determine the effects of gamma sterilization on the samples' isotopic, chemical, and physical properties. Gamma photons from ^{60}Co (1.17 and 1.33 MeV) in doses as high as 3×10^7 rads did not induce radioactivity in the samples and produced no measurable changes in their isotopic and chemical compositions. This level of irradiation also produced no measurable changes in the crystallographic structure of any sample, the surface areas of soil analogs, or the fluid inclusion homogenization temperature of quartz. The only detectable effects of irradiation were dose-dependent changes in the visible and near-infrared spectral region (e.g., discoloration and darkening of quartz and halite and an increase in albedo of carbonates) and increases in the thermoluminescence of quartz and plagioclase. If samples returned from Mars require biological sterilization, gamma irradiation provides a feasible option.

1. Background

Martian rock and soil, collected by robotic spacecraft, will be returned to terrestrial laboratories early in the next century. The return of documented samples, carefully collected and preserved, will be a major step in the search for evidence of Martian life. Martian conditions, including the lack of organic material, subfreezing temperatures, high flux of solar ultraviolet radiation, and strongly oxidizing chemical species in the soil, severely limit the survival of organisms at or near the surface [*Klein*, 1998]. However, terrestrial microorganisms have developed effective defenses against each of these stresses. The survival of specialized organisms at low concentrations in the returned samples is conceivable [*Clark*, 1998].

Current planetary protection strategies call for the samples to be immediately placed into biological containment and tested for signs of present or past life and biological hazard [*DeVincenzi et al.*, 1998]. It is recommended that "Controlled distribution of unsterilized materials from Mars should occur only if rigorous analyses determine that the materials do not constitute a biological hazard. If any portion of the sample is removed from containment prior to completion of these analyses it should first be sterilized" [*Space Studies Board*, 1997]. While sterilization of Mars samples may not be required, an acceptable method must be available before the samples are returned to Earth.

A variety of sterilization techniques have been used or proposed for spacecraft missions to Mars. These include dry heating to temperatures of 150°C or higher, heating in the presence of high-pressure steam, exposure to poisonous gases such as paraformaldehyde or propiolactone, exposure to hydrogen peroxide vapor or plasma, exposure to ultraviolet light, and exposure to gamma radiation. The technique of choice depends on the composition of the medium and the desired results [*Hochstein et al.*, 1974; *NASA*, 1978; *Gooding*, 1990].

The characteristics of the first returned Mars samples are dictated by spacecraft design. The samples will include soil and rock in as much variety as the landing site and the robotic acquisition system can support. NASA has selected a suite of analytical instruments and sample collecting devices for the first Mars sample return missions [*Squyres et al.*, 1998]. The package, named "Athena", features a cup-shaped collector which will acquire multiple soil samples, each approximately 1 cm^3 in volume. A core drill will collect intact rock samples with nominal dimensions of 8 mm (diameter) by 17 mm (length). Each specimen will be separately cached for return to Earth. A

[1]Lockheed Martin Space Operations, Houston, Texas.
[2]Montana Biotech Corporation, Belgrade, Montana.
[3]Department of Soil and Water Sciences, Hebrew University, Rehovot, Israel.
[4]Department of Geological Sciences, Virginia Polytechnic Institute and State University, Blacksburg, Virginia.
[5]Department of Geology, Arizona State University, Tempe, Arizona.
[6]Department of Earth and Planetary Sciences, Washington University, St. Louis, Missouri.
[7]NASA Johnson Space Center, Houston, Texas.
[8]Department of Natural Science, University of Houston -- Downtown, Houston, Texas.
[9]Department of Earth Sciences, Boston University, Boston, Massachusetts.
[10]Centers for Disease Control and Prevention, Atlanta, Georgia.
[11]University of Portsmouth, Portsmouth, England.

Paper number 1999JE001064.
0148-0227/99/1999JE001064$09.00

backup strategy calls for the collection of one or more contingency samples of mixed soil and pebbles. In any case, the sample mass is expected to total a few hundred grams, with the largest individual rocks approximately 2 cm in the longest dimension.

Mars samples returned by spacecraft may prove to be biologically sterile, in which case further sterilization will not be necessary. If sterilization of a subset of samples is required, however, the desired results are twofold. First, any viable organisms must be killed. Second, to the greatest extent possible, the isotopic, chemical, and physical characteristics of the rock and soil samples must be preserved. *Hochstein et al.* [1974] addressed some of the effects of sterilization on the organic geochemistry and morphology of returned samples. The predicted effects of various sterilization techniques on the full range of physical and chemical data were extensively discussed in polls of the planetary science community in 1974 [*Bogard et al.*, 1979] and again in 1987. *Gooding* [1990] summarized the findings of both polls and published all responses verbatim.

These studies and polls did not reach consensus on an optimal technique for sterilizing Mars samples. Each technique was predicted to compromise some portion of the samples' potential data return. Dry heating and steam heating, in particular, could result in irreversible degassing and strongly alter the structure of many primary and secondary minerals. Treatment with gas, vapor, plasma, or ultraviolet light would sterilize sample surfaces but would not fully penetrate into rocks. Several respondents suggested that exposure to high doses of gamma radiation might be the sterilization technique which would result in the least damage to rocks and soils [*Gooding*, 1990].

The current study investigates the effects of gamma radiation on geologic materials analogous to the first samples to be returned from Mars. We selected ^{60}Co radiation, which is widely used for sterilization in medical research and industrial processing. Total doses ranged from 3×10^5 to 1×10^8 rads (1 rad = 100 ergs/g), spanning the published sterilizing doses for bacteria and viruses. Twelve rock and mineral samples, chosen as possible Martian analogs, were irradiated. The effects of irradiation were measured by colleagues using a variety of techniques regularly employed to study terrestrial and extraterrestrial samples.

2. Previous Studies of Gamma Radiation Effects

2.1. Effects on Microorganisms

At sufficiently high exposure levels, ionizing radiation is lethal for all microorganisms. Radiation effects have been demonstrated in a number of sensitive cellular biomolecules including proteins and lipids but most notably DNA [*Battista*, 1997a]. Gamma radiation is routinely used for sterilization of medical supplies [*Moseley*, 1984] and samples in microbiological research [*Elliott et al.*, 1982]. Absorbed doses on the order of 10^6 rads are sufficient to destroy most of the microbes reported thus far and inactivate most viruses [*Battista*, 1997b].

The survival percentage of the common and well-studied bacterium *Escherichia coli* falls to 0.1% at a gamma dose of 1×10^5 rads [*Battista, 1997b*]. *Ledney et al.* [1996] reported 0.1% survival of *Bacillus subtilis* at 3×10^5 rads and *Bacillus pumilus* at 9×10^5 rads.

Deinococcus radiodurans is the most radiation-resistant bacteria yet reported. A strain of this species proved capable of growth in a flux of 6×10^3 rads/h in a ^{137}Cs irradiator [*Lange et al.*, 1998]. *D. radiodurans* exhibits no loss of viability at gamma doses as high as 6×10^5 rads but undergoes an exponential decline at higher doses. Its concentration in growing cultures falls to <0.1% of the starting value at a dose of 1×10^6 rads [*Battista*, 1997b].

Viruses exposed to sufficiently high gamma doses are inactivated, i.e. rendered incapable of causing infection. *Elliott et al.* [1982] demonstrated that doses of 7×10^5 rads are sufficient to inactivate *Ebola*, *Lassa*, and *Marburg* viruses to the 0.1% level at a temperature of 4°C. *Richmond and Walker* [1982] stated that, for the U.S. Department of Agriculture Plum Island facility, "6×10^6 rad has been selected as an irradiation dose level sufficient to inactivate completely any viral contaminates in frozen biological materials."

2.2 Effects of Desiccation and Cold

Radiation resistance in several species of bacteria is correlated with resistance to desiccation [*Mattimore and Battista*, 1995]. The type of DNA fragmentation induced by drying is similar to that caused by radiation, and bacterial DNA repair mechanisms are effective against both types of stress. Resistance to levels of radiation far exceeding those in the natural environment may be a secondary consequence of resistance to extreme desiccation.

The radiation resistance of some organisms in a frozen state also increases dramatically. As noted above, the viability of *D. radiodurans* in a growing culture at room temperature falls to <0.1% at a dose of 1×10^6 rads [*Battista*, 1997b]. At a temperature of -70°C, the same species exhibits 37% survival at a dose of 3×10^6 rads [*Daly et al.*, 1994].

If microorganisms exist on Mars, they have adapted to much colder and direr conditions than are common on Earth [*Klein*, 1998]. Such conditions are apparently correlated with high resistance to ionizing radiation. Thus sterilization of Martian microbes could require gamma doses significantly in excess of sterilizing doses for terrestrial organisms.

2.3 Nuclear and Chemical Effects

The irradiation experiments described below utilized ^{60}Co. Each atom of ^{60}Co that undergoes beta decay produces gamma rays with energies of 1.17 and 1.33 MeV. We investigated the interaction of this radiation with the nuclei and electrons of a variety of geologic materials.

While statistically improbable, it is possible for gamma rays to interact with atomic nuclei. If ^{60}Co gamma rays are absorbed by one of the 279 types of stable nuclei, by far the most likely outcome is that the excited state nucleus rapidly decays back to the ground state by emitting one or more gamma rays. A few nuclei, such as ^{117}Sn, have relatively long-lived isomeric states that can be detected by gamma counting after the irradiation ends [*Carroll et al.*, 1991]. This isotope, one subject of the current experiments, provides an extremely sensitive test of possible induced radioactivity.

Binding energies for the last nucleon in stable nuclei are typically in the range of 5 to 12 MeV. Binding energies for light elements of biological interest, including ^{2}H, ^{9}Be, ^{13}C, and ^{17}O, range from 1.7 to 4.9 MeV [*Lone*, 1990], all greater than the energy of a gamma photon from ^{60}Co. Thus radiation from ^{60}Co would not be expected to cause transmutations nor isotopic effects by ejection of nucleons.

2.4 Electron Shell Effects

As radiation in the MeV energy range passes through matter, most of the energy loss is to orbital electrons by the process of Compton scattering. A gamma photon loses a portion of its

energy, typically several hundred eV, with each interaction. The most probable effects of irradiation involve the displacement or excitation of electrons. In minerals these effects are manifested as changes in color and thermoluminescence.

One well-known effect of gamma irradiation is the darkening and coloration of certain sensitive glasses and minerals (e.g., quartz [*Shulman and Compton*, 1962]) through the creation of color centers. The creation of colloidal element concentrations in irradiated metal halides can also lead to color changes [*Pederson*, 1985].

The production of thermoluminescence occurs when previously excited electrons are thermally released from electron "traps" and luminesce while returning to the ground state. The excitation source, which can be one of several forms of ionizing radiation, excites an electron from the valence band to the conduction band. Traps are often described as impurity ions, lattice vacancies or dislocations. Many different minerals exhibit TL, including quartz, phosphates, carbonates, enstatite and feldspar [*McKeever and Sears*, 1979].

2.5 Effects on Rocks and Minerals

A limited number of studies have been published concerning the effects of high gamma radiation doses on rocks and minerals. Much of this research was directed toward understanding the interactions of nuclear waste with various containers, packing materials and geologic environments.

Spitsyn et al. [1981] subjected feldspars and quartz to ^{60}Co gamma radiation. They reported color changes in the feldspars, minor loss of crystallinity and shifts in some infrared spectral peaks. These effects were initiated at doses of 10^7 to 10^8 rads.

Krumhansl [1986] exposed montmorillonite clay to ^{60}Co gamma doses as high as 3×10^{10} rad. X-ray diffraction data indicated no significant changes. Heat capacity measurements showed loss of interlayer water to be the only crystallographic effect. *Allen and Rawson* [1986] studied montmorillonite which had been exposed to 3.5×10^9 rads of ^{60}Co gamma radiation and at the same time heated to 300°C. The only observed change was reversible loss of interlayer water. *Spitsyn et al.* [1982] characterized a range of clays subjected to gamma doses ranging from 10^7 to 10^9 rads. They reported no structural changes other than partial dehydration.

Pederson [1985] described results from gamma irradiation of natural rock salts and synthetic NaCl at doses of 10^8 to 10^9 rads and temperatures of 50° to 150°C. At the lower temperatures the salts turned dark blue, which the author ascribed to the formation of sodium colloids. Salts from the higher temperature experiments became light brown, a color typical of anion vacancies containing trapped electrons. Heating of the samples to 190°C caused the recombination of radiation-induced defects. *Jockwer and Monig* [1989] studied the gases released by irradiated samples of rock salt. They reported significant levels of CO_2 and CO, produced by desorption, and N_2O from radiolysis of air.

2.6 Shielding

Compton scattering of gamma rays by electrons shows an exponential dependence on thickness of the form:

$$I = I_0 e^{-\mu d} \quad (1)$$

where I_0 is the incident intensity, I is the transmitted intensity after passing through an absorber of thickness d, and μ is the mass absorption coefficient, which is related to the material's density and the photon's energy. Shielding capacity is quantified as a "half-thickness", i.e. the amount of material required to reduce I/I_0 to 0.5. For 1.33 MeV gamma photons, the half-thickness for a wide range of materials is approximately 13 g/cm^2 [*Friedlander et al.*, 1964]. This is equivalent to a 4.6 cm thick layer of basalt (density 2.8 g/cm^3 [*Basaltic Volcanism Study Project (BVSP)*, 1981]). Thus the 8 x 17 mm rock cores and the 1 cm^3 splits of soil which will constitute the first returned Mars samples should provide less than 6% shielding. These small samples will be essentially transparent to sterilizing gamma radiation.

3. Sample Preparation and Irradiation

3.1 Rocks and Minerals

All sample preparation for the current study was done at the NASA Johnson Space Center (JSC). Fourteen materials were prepared for gamma irradiation: basalt, quartz, plagioclase, olivine, pyroxene, phyllosilicate, Mars soil simulant, carbonaceous chert, carbonaceous chondrite meteorite, halite, aragonite, gypsum, water, and tin (Table 1). The phyllosilicate (fine powder), Mars soil simulant (<1 mm powder), tin (3 to 4 g blocks), and water were used without specific preparation. Other samples were subdivided into three size fractions: single crystals or chips 0.5 to 1 cm in length, <1 mm powders, and <0.1 mm powders. These latter two splits were prepared by grinding in a tungsten carbide shatterbox. All grinding was done dry, although the aragonite sample was found to be significantly wet following grinding.

For irradiation experiments, approximately 1 cm^3 of each split was placed in a snap-top plastic vial. Sets of each material were prepared for each radiation dose, and an identical set was prepared as an unirradiated control. In one irradiation experiment, three large quartz crystals (2.5 cm in width) were exposed. For fluid inclusion studies, polished plates of quartz were prepared as described below. Fluid inclusions were analyzed in the quartz before irradiation, and the same inclusions were reanalyzed after irradiation.

3.2 Irradiation

Three rounds of irradiation experiments were conducted in a Gammacell 220 High Dose Research Irradiator (MDS Nordion) at the Centers for Disease Control and Prevention. The unit was loaded with approximately 24,000 curies of ^{60}Co in February 1998. At that time the gamma dose rate, calibrated using Fricke dosimetry [*American Society for Testing and Materials (ASTM)*, 1997), was established to be 3.15×10^4 rads/min. The total gamma dose in each experiment was determined by the length of time the sample set remained in the irradiator.

The samples were exposed at ambient temperatures. Water samples showed no evidence of boiling, indicating a sample temperature below 100°C. A representative of the manufacturer estimated that the chamber temperature did not exceed 49°C.

The first round of irradiation was conducted in March 1998. Triplicate splits of all 14 rock and mineral samples were exposed. Irradiation durations of 9.5, 95, and 950 min corresponded to total doses of 3×10^5, 3×10^6 and 3×10^7 rads, respectively. For the second round of irradiation, in May 1998, eight materials were used: basalt quartz, plagioclase, phyllosilicate, Mars soil simulant, halite, gypsum, and water. Powders, along with single crystals of quartz and halite, were prepared and packaged in triplicate sets (along with one control set) as described above for irradiation at 3×10^7 and 1×10^8 rads. A third round of irradiation, conducted in August 1998, exposed several large quartz crystals to 3×10^7 rads.

Table 1. Rock and Mineral Samples

Sample	Description
Basalt	Fine-grained tholeiite (plagioclase, pyroxene), 14 Ma, Umtanum flow of Grande Ronde Formation, Columbia River Basalt Group, Hanford, Washington [*BVSP*, 1981]
Quartz	SiO_2 (trace anhydrite), Mt. Ida, Arkansas
Plagioclase	Labradorite, Lake County, Oregon [*Stewart et al.*, 1966]
Olivine	Forsterite, San Carlos, Arizona
Pyroxene	Diopside, Hull, Quebec
Phyllosilicate	Na-montmorillonite (SWY-1 Wyoming bentonite), Source Clays Repository, University of Missouri [*Van Olphen and Fripiat*, 1979]
Mars soil simulant	JSC Mars-1, weathered volcanic ash (hydrated glass, plagioclase, Ti-magnetite, minor pyroxene, olivine), Hawaii [*Allen et al.*, 1998]
Carbonaceous chert	Stromatolite facies (calcite, quartz, dolomite, greenalite, minor ankerite, siderite, minnesotaite), 1.9 Ga, Gunflint Formation, Thunder Bay, Ontario [*Carrigan and Cameron*, 1991]
Carbonaceous chondrite	ALH83100, CM2, highly altered (Fe-rich phyllosilicates, calcite, Fe-oxides) [*MacPherson*, 1985]
Halite	99.5% NaCl (trace clay, gypsum, polyhalite, calcite), Waste Isolation Pilot Plant drill core VS04, Carlsbad, New Mexico
Aragonite	Narrow Gauge spring, Yellowstone National Park, Wyoming [*Chafetz and Lawrence*, 1994]
Gypsum	Grand Rapids, Michigan
Water	Deionized, <0.2 μm filtered
Tin	Standard 42f, National Institute of Standards and Technology

Quartz samples for the fluid inclusion study were irradiated in the Phoenix Memorial Laboratory ^{60}Co facility at the University of Michigan. The peak dose rate in the irradiator was approximately 3 x 10^4 rads/min. The samples received a total dose of 3 x 10^7 rads.

4. Analytical Methods and Procedures: Effects of Radiation on Rocks and Minerals

The control and irradiated rock and mineral samples were analyzed by a variety of techniques to assess irradiation effects. The techniques and the samples analyzed by each are listed in Table 2.

4.1 Gamma Ray Spectroscopy

Each combined set of samples (irradiated as high as 3 x 10^7 rads) was monitored for induced radioactivity in the JSC Radiation Counting Laboratory. Gamma ray counting systems include two large intrinsic Ge detectors (EG&G Ortec) selected for high resolution (1.8 keV at 1.332 MeV) and mounted in low-background cryostats which extend into Pb shields lined with Cd and Cu. Data reduction is done using programs based on TEABAGS [*Lindstrom and Korotev*, 1982]. Counting was conducted approximately 72 hours after the completion of irradiation. Combined sample sets were placed in the counter together and counted for 48 hours. The tin samples were counted separately.

4.2 Isotope Analysis and Age Dating

The ratios of $^{87}Sr/^{86}Sr$, $^{149}Sm/^{152}Sm$, and $^{150}Sm/^{152}Sm$ were measured for unirradiated and irradiated (3 x 10^7 rads) basalt, carbonaceous chert, and carbonaceous chondrite samples. Measurements were conducted in the JSC Thermal Ionization Mass Spectrometry Laboratory using standard procedures for radiometric age dating [*Nyquist et al.*, 1994].

Wide variations in isotope ratios measured for the carbonaceous chert and carbonaceous chondrite samples indicated that they were chemically heterogeneous, making the comparison of data meaningless. Only the fine-grained basalt was sufficiently homogeneous to provide reliable results.

4.3 Instrumental Neutron Activation Analysis (INAA)

Selected major, minor, and trace element abundances in powdered basalt and Mars soil simulant were measured in the INAA laboratory at JSC. Splits of approximately 50 mg mass were taken from the control sample and material exposed to 3 x 10^5, 3 x 10^6, and 3 x 10^7 rads. All samples were heated to 400°C in air for 12 hours to remove adsorbed and bound water.

The samples, standards, and unirradiated controls were encapsulated in pure SiO_2 glass tubes and irradiated at the Research Reactor Facility of the University of Missouri for 12 hours at a thermal neutron flux of 5.5 x 10^{13} n cm^{-2} s^{-1}. The samples were counted three times roughly ½, 1, and 4 weeks after irradiation in order to obtain data for nuclides of differing half-lives. The counting system used intrinsic Ge detectors and fed the spectral data into a multichannel analyzer using 8192 channels with the energy calibration set to 0.25 keV per channel. Details of the standards used, data reduction process, and correction procedures can be found in the work by *Mittlefehldt and Lindstrom* [1993] and references therein.

The Mars soil simulant, a complex multiphase mixture with grains as large as 1 mm, proved too heterogeneous for meaningful comparisons among 50 mg samples. Usable data were obtained from the powdered basalt.

4.4 Inductively Coupled Plasma Emission Spectrometry (ICP-ES)

Major, minor, and trace element concentrations in powdered basalt, aragonite, carbonaceous chert, phyllosilicate, gypsum, halite, Mars soil simulant, and pyroxene samples were measured in the Analytical Geochemistry Laboratory at Boston University. The sample set included unirradiated controls and samples exposed to 3 x 10^7 rads. The sample preparation procedure was similar to that of *Murray and Leinen* [1996]. Solutions were introduced by conventional Meinhard nebulization into a Jobin-Yvon JY170C combined sequential and simultaneous ICP-ES and analyzed in comparison to matrix-matched synthetic standards.

Table 2. Analyses of Rock and Mineral Samples

Sample	Gamma Ray Spectroscopy	Sr, Sm Isotopes	INAA	ICP-ES	Micro-probe	XRD	TES	Raman	SSA	Fluid Inclusions	VIS/NIR	TL
Basalt	X	X	X	X		X					X	X
Quartz	X				X	X		X		X	X	X
Plagioclase	X					X		X			X	X
Olivine	X					X		X			X	
Pyroxene	X			X		X	X				X	
Phyllosilicate	X			X		X			X		X	
Mars soil simulant	X		X	X		X	X		X		X	X
Carbonaceous chert	X	X		X		X					X	
Carbonaceous chondrite	X	X				X					X	X
Halite	X			X		X	X				X	
Aragonite	X			X		X	X	X			X	
Gypsum	X			X		X	X	X			X	
Tin	X											

Blanks, internal references, and international Standard Reference Materials (SRMs) were run. Every solution, regardless of type, was analyzed in triplicate. Relative standard deviations ($\pm 1\sigma$) of the triplicate analyses of each solution were at most 2% and commonly less 0.5% of the measured values. Analytical detection limits were calculated as $\pm 3\sigma$ of the average of three blank solution analyses.

Precision of the entire analysis was determined from replicate preparation (i.e., from the powder weighing step onward) and analyses of SRM MAG-1 (U.S. Geological Survey; marine sediment from the Gulf of Maine) and of other natural samples. Accuracy was assessed by comparison of the results of the analysis of MAG-1 to accepted values. Data for all elements were in agreement with the accepted values, with the exception of Na, Mg, and Ba, which appeared to be slightly systematically low (by 5 to 10% of the measured values). The absolute concentrations of Cr were in disagreement by approximately 25% of the measured value.

4.5 Electron Microprobe Analysis

Selected minor and trace element distributions in an irradiated (3×10^7 rads) quartz crystal were measured on a Cameca SX 100 electron microprobe at JSC. A polished section was carbon-coated and analyzed at an accelerating potential of 15 kV and a beam current of 200 nA.

4.6 X-Ray Diffraction (XRD)

The crystal structures of all samples except tin and water were analyzed by powder XRD at JSC. In each case the previously ground fine powder (<0.1 mm) split was employed, except for the Mars soil simulant and phyllosilicate, which were measured "as received." Control samples and samples exposed to 3×10^7 rads were prepared by pressing the powders into aluminum sample holders. The powders were analyzed in a Scintag XDS 2000 X-ray diffractometer using Cu-kα radiation.

Dominant (relative intensity ≥10%) peaks for the minerals were identified by reference to the Mineral Powder Diffraction File [*JCPDS*, 1980]. Lattice spacings for these peaks in both irradiated and control splits of all samples were compared. Changes in peak widths were assessed by overlaying plots of XRD spectra.

4.7 Thermal Emission (Vibrational) Spectroscopy (TES)

Thermal emission spectra of 14 samples of five geologic materials (<1mm splits of halite, pyroxene, aragonite, and gypsum, as well as Mars soil simulant) were acquired over the range 5 to 25 μm. The analyses were performed on a Mattson Cygnus 100 Fourier transform infrared spectrometer at the Thermal Emission Spectrometer Laboratory at Arizona State University. The instrument and details of its calibration are described by *Ruff et al.* [1997]. The pyroxene and gypsum suites each comprised one control sample (unirradiated) and three samples variously irradiated at 3×10^5 rads, 3×10^6 rads, and 3×10^7 rads. The halite, aragonite, and Mars soil simulant suites each comprised a control and a single sample irradiated at 3×10^7 rads.

Samples were heated overnight at 80°C in order to increase the thermal radiance of the samples at the time of data acquisition. Each spectrum was the average of 200 scans (approximately 330 s acquisition time) and had a spectral sampling of 2 cm^{-1}. Each sample was heated throughout the data acquisition period to eliminate cooling effects in the data. The data were calibrated to remove instrument response and were converted from radiance to emissivity via the one-temperature method of *Ruff et al.* [1997], derived from the two-temperature method of *Christensen and Harrison* [1993].

Because of the unsorted nature of the samples, the distribution of particle sizes among splits of the same composition is unlikely to be the same, resulting in variable particle size effects in the spectra of the splits (e.g., variable band depths). Absorption features in all of the spectra due to terrestrial atmospheric water vapor are present at wavelengths between 6 and 7 μm. The intensities of these features are sensitive to atmospheric conditions at the time of data acquisition.

4.8 Raman Spectroscopy

Control and irradiated (3 x 10^7 rads) splits of plagioclase, olivine, aragonite, quartz, and gypsum (single chips or <1 mm powders) were measured. This study utilized the HoloLab-5000-633 Raman spectrometer system (Kaiser Optical Systems Inc.) located at Washington University.

The system consists of a Raman probe coupled with a microscope for sampling and a spectrograph with a laser source. This configuration simultaneously provides wide spectral coverage (-177 to 4017 cm^{-1}) with high spectral resolution (4 to 5 cm^{-1}), and high light throughput. A two-dimensional (1024 by 256 pixel) charge-coupled device is used as the multichannel detector, and the 632.8 nm line of a He-Ne laser is used for excitation. Mineral or rock samples are placed directly on the microscope stage with no sample preparation. A microscope objective condenses and directs the excitation laser beam onto the sampling spot. Raman-scattered radiation is collected and returned to the spectrograph through the same objective.

A 20x long working-distance objective (0.4 numerical aperture) produced a condensed laser beam approximately 2 μm in diameter at the focusing plane. The laser power at the sample spot was approximately 9 mW, and no sample overheating was observed. The wavelength reading of the spectrograph was calibrated according to the emission lines of a standard Ne source. Spectra were measured on a Si wafer before and after the experiments; no wavelength shifts were observed. The background of each spectrum obtained in this study was corrected using the overall response curve of the Raman system.

All samples were analyzed using the same conditions (5 s integration time and six accumulations per spectrum). Two spectra from each sample were acquired in the initial survey to exclude variations due to sample inhomogeneity. Analysis spots were chosen in flat areas on grain surfaces to maximize signal, but no effort was made to orient grains. In cases where variations were observed that could potentially be correlated to irradiation level, additional spectra were obtained to test that possibility.

4.9 Specific Surface Area

Key surface parameters of the returned Mars soil may be affected by proposed sterilization protocols. A basic property in this context is the specific surface area (SSA, m^2 per g of mineral) of the powdered soil. SSA is related to fluid and gas sorption capacities of the soil and to its overall reactivity in various processes. Measurement of specific surface area is conducted by using either nonpolar molecules such as N_2 [*Kantro et al.*, 1967] or polar molecules, usually glycols and their derivatives [*Carter et al.*, 1965; *Ratner-Zohar et al.*, 1983].

Specific surface areas of Mars soil simulant and phyllosilicate samples were measured at Hebrew University. SSA was calculated from sorption of ethylene glycol monoethyl ether (EGME) following the method of *Ratner-Zohar et al.* [1983]. The polar probe molecule used in this method has higher penetration ability than the nonpolar N_2 and is better correlated with, and thus more informative on, the behavior of water molecules and their interactions at the mineral surface.

Weighed samples (control and irradiated to 3 x 10^7 rads) were dried for 24 hours at 105°C, and the weight losses were determined. Excess EGME was added, and each sample was placed in a desiccator above dry $CaCl_2$. After equilibration for 2 hours, the wet samples were exposed to high vacuum (approximately 0.1 mm Hg) for 16 hours, and then retained under these conditions for 48 hours, to obtain monolayer coverage of EGME on the mineral surfaces. The samples were then weighed again. The specific surface area of each sample was calculated from the added weight assuming that 2.86 x 10^{-4} g of EGME covered 1 m^2 of surface as a monolayer. A standardized mineral sample (purified smectite/Na-montmorillonite from Wyoming) was included throughout the procedure.

4.10 Fluid Inclusions

In order to determine whether gamma sterilization might affect the fluid inclusions contained within mineral samples, the same group of fluid inclusions in quartz was analyzed before and after irradiation (3 x 10^7 rads). The analyses were conducted in the Fluids Research Laboratory at Virginia Tech. A single 2.5-cm-wide crystal was cut perpendicular to the C axis, and two doubly polished plates a few millimeters thick were prepared. A total of 55 fluid inclusions (13 in one plate and 42 in the second plate) were selected for analysis. Inclusion sizes ranged from about 50 μm down to the limits of optical resolution (approximately 1 μm); morphologies ranged from irregular to negative-crystal shaped. Each inclusion was heated using a modified U.S. Geological Survey (USGS)-type, gas-flow heating/cooling stage to measure the liquid-vapor homogenization temperature (TH) before irradiation. The inclusions were photographed, and a map was prepared so that the same inclusions could be located and measured after irradiation.

When a crystal forms in the presence of a fluid phase (liquid, vapor or melt), some of the fluid may be trapped as defects in the growing crystal to form primary fluid inclusions [*Roedder*, 1984]. Similarly, if the crystal fractures either during or after formation, fluids may enter the fracture and become trapped as pseudosecondary or secondary inclusions, respectively, as the fracture heals. Fluid inclusions thus contain microsamples of the fluids that were present during and/or following crystal formation and provide a direct means of determining the temperatures of mineral formation and the compositions of fluids responsible for mineralization.

When observed at room temperature, most fluid inclusions contain two or more phases. The most common inclusion type contains liquid and vapor phases at room temperature. The vapor bubble forms when the liquid phase originally trapped at elevated temperatures shrinks (becomes more dense) during cooling, while the "crystal bottle" containing the fluid remains isochoric (constant volume). Similarly, if the trapped fluid contains high concentrations of dissolved components, the fluid in the inclusion may become saturated in one or more solid phases during cooling, and precipitate daughter minerals in the inclusion. During microthermometric analysis, the inclusions are heated while being observed under a microscope, and the temperatures at which the various phases disappear are recorded. The temperature at which the last two phases in the inclusion homogenize into a single phase is referred to as the homogenization temperature and represents a minimum temperature of formation of the inclusion (and therefore the host mineral, if the inclusions are primary).

All of the inclusions analyzed in this study contained liquid and vapor at room temperature. During heating, the vapor bubble became smaller and disappeared at the homogenization temperature. The total range in TH for the 55 inclusions was

Table 3. Effects of Gamma Radiation on Isotope Ratios in Basalt

Dose, rads	$^{87}Sr/^{86}Sr$	$^{149}Sm/^{152}Sm$	$^{150}Sm/^{152}Sm$
Control	0.705542 ± 12	0.516853 ± 11	0.275978 ± 13
3 x 10^7	0 705546 ± 12	0.516843 ± 11	0.275979 ± 13

Uncertainties in last two significant figures ±2σ.

157.4°C to 164.1°C; the temperature measurements were accurate to ±1.0°C.

4.11 Visible and Near-Infrared (VIS/NIR) Reflectance Spectroscopy

Visible and near-infrared diffuse reflectance spectra (350 to 2100 nm) of the 12 rock and mineral powders (<0.1 μm except for phyllosilicate and Mars soil simulant) were collected on a Cary-14 spectrophotometer at JSC. The instrument was configured with a 9-inch-diameter integrating sphere and a microprocessor-based acquisition system. Samples were equilibrated with dry nitrogen gas for approximately 60 min prior to measurement and run at a temperature of 20°C. Halon was used as the reflectivity standard, and absolute reflectivities were calculated using the data of *Weidner and Hsia* [1981]. Control and irradiated samples receiving doses ranging from 3 x 10^5 through 1 x 10^8 rads were analyzed. Samples which formed clods during irradiation (especially quartz, aragonite, halite, and carbonaceous chert) were gently crushed to approximately restore their original textures.

4.12 Thermoluminescence (TL)

A study was carried out at the University of Arkansas to examine the effects of gamma radiation dose on the TL properties of rocks and minerals. Samples included control and irradiated (3 x 10^5 to 1 x 10^8 rads) powdered basalt, carbonaceous chondrite, plagioclase, quartz, and Mars soil simulant.

In the present study, 4 mg aliquots of sample were placed in shallow copper pans. Thermoluminescence data were collected by heating samples from ambient temperature to 500°C at a constant rate of 7.5°C/s in a nitrogen atmosphere. The light emitted was collected with an EMI 9635B photomultiplier tube (PMT) and recorded as a function of temperature. Corning 7-59 and 4-69 optical filters were placed in the light path of the PMT to restrict measurement to the wavelength range of 350 to 500 nm. After the natural TL was drained, each sample was given a known dose of radiation using a 250 mCi ^{90}Sr beta source, thus artificially filling the electron traps, and the thermoluminescence was measured again. Each sample was run in triplicate, with the data being averaged.

The TL data from controls and irradiated samples were reduced by measuring glow curve (light intensity versus temperature) parameters related to the physical nature of the phosphor. The TL sensitivity refers to the intensity of light produced after exposure to the ^{90}Sr source and is a measure of how responsive a material is to ionizing radiation.

Table 4. Effects of Gamma Radiation on Basalt Composition Measured by INAA

Element/ Oxide	Control	Abundance* 3 x 10^5 rads	3 x 10^6 rads	3 x 10^7 rads
Na_2O	3 23 ± 0.08	3.20 ± 0.08	3.19 ± 0.08	3.19 ± 0.08
K_2O	1.68 ± 0.14	1.72 ± 0.24	1.66 ± 0.20	1.71 ± 0.16
CaO	6.1 ± 1.0	7.1 ± 0.8	6.6 ± 0.8	6.8 ± 1.0
Sc	33.8 ± 0.8	33.8 ± 0.8	33.7 ± 0.8	33.7 ± 0.8
Cr	7.5 ± 1.0	7.1 ± 1.0	7.1 ± 1.0	6.8 ± 1.2
FeO	12.54 ± 0.28	12.54 ± 0.28	12.46 ± 0.28	12.43 ± 0.28
Co	54.2 ± 1.2	53.3 ± 1.2	53.3 ± 1.2	53.0 ± 1.2
As	1.03 ± 0.46	1.13 ± 0.32	1.07 ± 0.36	1.01 ± 0.30
Rb	52 ± 6	52 ± 6	51 ± 8	50 ± 4
Sr	284 ± 48	301 ± 50	273 ± 52	306 ± 58
Zr	200 ± 80	190 ± 60	190 ± 60	180 ± 60
Sb	0.151 ± 0.054	0.165 ± 0.038	0.154 ± 0.040	0.146 ± 0 042
Cs	1.34 ± 0.10	1.28 ± 0.08	1.28 ± 0.10	1.31 ± 0.12
Ba	593 ± 40	603 ± 34	597 ± 38	600 ± 44
La	24.89 ± 0.58	24.59 ± 0.56	24.69 ± 0.56	24.64 ± 0.56
Ce	53.9 ± 1.6	53.3 ± 1.6	52.9 ± 1.6	52.0 ± 1.6
Nd	30 ± 8	34 ± 6	32 ± 6	28 ± 8
Sm	6.94 ± 0.20	6.74 ± 0.18	6.80 ± 0.20	6.79 ± 0.20
Eu	2.05 ± 0.06	2.04 ± 0.06	2.02 ± 0.06	2.00 ± 0.06
Tb	1.173 ± 0.050	1.153 ± 0.044	1.149 ± 0.048	1.132 ± 0.052
Yb	3.75 ± 0.14	3.69 ± 0.14	3.68 ± 0.14	3.65 ± 0.14
Lu	0.554 ± 0.030	0.543 ± 0.024	0.538 ± 0.026	0.537 ± 0.026
Hf	5.53 ± 0.24	5.54 ± 0.22	5.52 ± 0.22	5.50 ± 0.24
Ta	1.59 ± 0.08	1.58 ± 0.08	1.55 ± 0.08	1.54 ± 0.08
W	205.5 ± 5.6	192.2 ± 4.6	196.0 ± 4.8	195.7 ± 4.8
Au	13.3 ± 5.2	13.7 ± 2.6	6.6 ± 3.2	6.8 ± 3.2
Th	5.46 ± 0.18	5.42 ± 0.16	5.37 ± 0.18	5.32 ± 0.18
U	1.60 ± 0.34	1.68 ± 0.20	1.61 ± 0.22	1.56 ± 0.20

*Oxide abundances in wt%; Au in ng/g; remainder in μg/g; uncertainties ±2σ.

Table 5. Effects of Gamma Radiation on Rock and Mineral Composition Measured by ICP-ES

Element	Basalt		Aragonite		Carbonaceous Chert		Phyllosilicate		Gypsum	
	Control	3 x 10^7 rads	Control	3 x 10^7 rads	Control	3 x 10^7 rads	Control	3 x 10^7 rads	Control	3 x 10^7 rads
P	1,680	1,600	14	10	524	512	199	200		
Fe	99,100	94,800	82	66	39,100	40,000	25,300	25,600		
Mn	1,640	1,630			8,680	8,680	99	102		
Al	70,100	70,400			2,540	2,580	95,500	96,000		
Ti	15,000	15,300			207	214	701	679		
Ca	53,700	52,300	405,000	401,000	258,000	254,000	12,500	12,700	25,400	25,200
Mg	19,800	19,700	136	127	65,900	64,100	14,500	15,000	143	128
Na	20,600	19,600	521	561	404	342	8,550	8,820	147	143
K	9,820	9,530					2,780	2,730		
Zn	133	132			10	10	76	75		
Ni	14	14			57	56	2	2		
Ba	567	562	73	73	70	67	119	118		
Cr	10	10			14	11	2	2		
V	296	291			96	98	4	3		
Cu										
Zr	229	226	5	5	15	15	162	161	5	5
Sr	306	304	1,580	1,580	112	112	277	279	185	182

Element	Halite		Mars Soil Simulant		Pyroxene		Wavelength, nm	Detection Limit, %	Precision, %
	Control	3 x 10^7 rads	Control	3 x 10^7 rads	Control	3 x 10^7 rads			
P			2,730	2,780			177.440	10	2.3
Fe			87,400	89,900	15,000	14,500	238.204	1.5	2.6
Mn			1,710	1,690	1,460	1,450	257.610	0.3	0.9
Al			93,800	94,000	11,800	11,800	308.215	80	0.9
Ti			19,800	19,400	141	135	308.802	5	1.8
Ca	422	439	38,500	39,000	173,000	171,000	317.933	10	1.6
Mg	44	59	21,200	22,000	90,900	90,500	383.826	25	1.4
Na	302,000	300,000	12,700	12,700	6,420	6,620	588.995	2	1.9
K	193	173	3,800	3,660	1,530	1,570	766.490	5	2.6
Zn			106	106	120	120	213.856	0.1	4.7
Ni			69	73	17	14	231.604	0.6	1.4
Ba			424	419	42	43	233.527	0.1	1.0
Cr			103	138	3	2	267.716	0.3	0.6
V			106	110	13	13	310.230	0.2	0.7
Cu			2	4			324.754	0.1	2.6
Zr	5	5	467	468	13	11	343.823	0.2	4.4
Sr	2	2	907	904	82	82	407.771	0.01	0.5

All abundances in ppm; relative standard deviations (±1σ) of triplicate analyses, <2% of measured values; all data specified to three significant figures.

Table 6. Effects of Gamma Radiation on Unit Cell Parameters Measured by XRD

hkl	PDF (A)	Ctrl (A)	Irrad (A)	Irrad/Ctrl
		*Plagioclase (Anorthite 10-360)**		
020,110	6.49	6.408	6.415	1.001
021	4.68	4.646	4.660	1.003
201	4.03	4.022	4.018	0.999
111	3.90	3.880	3.879	1.000
111	3.75	3.739	3.740	1.000
131	3.63	3.617	3.619	1.000
112	3.46	3.457	3.455	0.999
112	3.36	3.350	3.350	1.000
220	3.23	3.224	3.222	1.000
040,202	3.20	3.197	3.190	0.998
002	3.17	3.168	3.168	1.000
220	3.13	3.120	3.121	1.000
131	3.02	3.016	3.014	0.999
041	2.94	2.938	2.939	1.000
132	2.65	2.645	2.644	0.999
112	2.51	2.509	2.513	1.002
		*Pyroxene (Diopside 11-654)**		
021	3.35	n.d.	3.332	
220	3.23	3.218	3.220	1.000
221	2.991	2.977	2.980	1.001
310	2.952	2.939	2.941	1.001
311	2.893	2.882	2.884	1.001
131	2.566	2.556	2.558	1.001
112,221	2.518	2.508	2.510	1.001
311	2.304	2 297	2.297	1.000
330	2.157	2.149	2.150	1.000
331	2.134	2.127	2.128	1.001
202	2.009	2.008	2.010	1.001
150	1.755	1.750	1.751	1.000
223,531	1.625	1.622	1.623	1.000
		*Olivine (Forsterite 7-159)**		
020	5.15	5.067	5.078	1.002
021	3.916	3.866	3.872	1.002
101	3.744	3.704	3.711	1.002
120	3.481	3.474	3.475	1.000
002	3.014	2.982	2.987	1.002
130	2.791	2.761	2.763	1.001
131	2.533	2.507	2.509	1.001
112	2.475	2.452	2.457	1.002
041	2.370	2.343	2.347	1.002
122	2.285	2.265	2.268	1.001
140	2.270	2.245	2.247	1.001
		*Gypsum (6-46)**		
020	7 56	7 491	7 495	1.001
121	4.27	4.248	4.248	1.000
031,040	3.79	3.774	3.775	1.000
141	3.059	3.048	3.049	1.000
002	2.867	2.857	2.858	1.000
022,051	2.679	2.671	2.672	1.000
123	2.080	2.077	2.078	1.000
080,062	1.898	1.894	1.894	1.000
143	1.879	1.874	1.875	1.000
262	1.812	1.807	1.807	1.000
260	1.778	1.773	1.774	1.001
		*Quartz (5-490)**		
100	4.26	4.205	4.185	0.995
101	3.343	3.315	3.299	0.995
110	2.458	2.441	2.435	0.997
102	2.282	2.269	2.263	0.997
111	2.237	2.225	2.219	0.997
200	2.128	2.117	2.112	0.998
201	1.980	1.970	1.967	0.999
112	1.817	1.811	1.807	0.998
202	1.672	1.666	1.663	0.998
		*Aragonite (5-453)**		
111	3.396	3.371	3.365	0.998
021	3.273	3.251	3.245	0.998
012	2.700	2.686	2.683	0.999
200	2.481	2.470	2.468	0.999
031	2.409	2.398	2.395	0.999
112	2.372	2.361	2.358	0.999
130	2.341	2.330	2.326	0.999
211	2.188	2.181	2.178	0.999
220	2.106	2.097	2.095	0.999
221	1.977	1.970	1.968	0.999
041	1.882#	1.874	1.872	0.999
202	1.877#	n.d.	1.862	
132	1.814	1.809	1.807	0.999
113	1.742	1.737	1.736	0.999
231	1.728	1.721	1.720	0.999

5. Results

5.1 Effects of Radiation on Rocks and Minerals: Induced Radioactivity and Isotopic Structure

5.1.1 Gamma ray spectroscopy. The combined sample set exposed to 3 x 10^5 rads produced 36 gamma ray peaks, all attributable to natural K, Th, and U in the samples or to traces of ^{137}Cs produced by atmospheric nuclear tests. The net count rate attributable to these peaks across the energy range 0.05 to 2.0 MeV was 0.521 ± 0.003 counts/s (±2σ). The sample set exposed to 3 x 10^7 rads produced the same 36 gamma peaks and an identical net count rate. Thus the combined sample sets showed no detectable evidence of induced radioactivity.

Samples of tin were irradiated to monitor the production of ^{117m}Sn, a gamma emitter with a half-life of 13.6 days [*Carroll et al.*, 1991]. Following a radiation dose of 3 x 10^7 rads, a 3.64 g sample of tin showed no detectable counts above background, at a sensitivity of 0.004 counts/s (±2σ). This count rate sets an extremely low upper limit of <7000 atoms of ^{117m}Sn created, corresponding to <5x10^{-18} of the ^{117}Sn atoms present.

5.1.2 Isotope analysis and age dating. Table 3 presents the effects of gamma radiation on isotope ratios in the fine-grained Columbia River basalt. The ^{87}Sr/^{86}Sr ratios of control and irradiated (3 x 10^7 rads) samples were indistinguishable within the ±2σ error limits of the analysis.

The Columbia River basalts are geologically young (approximately 14 Ma [*BVSP*, 1981]) and thus have nearly constant ^{87}Sr/^{86}Sr throughout, independent of the Rb/Sr ratio. The unirradiated and irradiated basalt splits have identical measured ^{87}Sr/^{86}Sr ratios. Thus a basalt's measured ^{87}Rb-^{87}Sr age should remain unchanged following 3 x 10^7 rads of gamma irradiation.

Table 6. (continued)

hkl	PDF (A)	Ctrl (A)	Irrad (A)	Irrad/Ctrl
		Basalt		
		3.9943	4.0119	1.004
		3.7117	3.7262	1.004
		3.6053	3.6214	1.004
		3.3338	3.3468	1.004
		3.1806	3.1909	1.003
		3.1523	3.1636	1 004
		3.1107	3.1214	1.003
		2.9785	2.9873	1.003
		2.9166	2.9271	1.004
		2.9052	2.9146	1 003
		2.8894	2.8897	1.000
		2.5555	2.5608	1.002
		2.5397	2.5458	1.002
		2.5028	2.5112	1.003
		2.4888	2.4953	1.003
		2.1287	2.1334	1.002
		2.1088	2.1146	1.003
		1.6228	1.6259	1 002
		Mars Soil Simulant		
		3.992	3.996	1.001
		3.720	3.724	1 001
		3.622	3.608	0.996
		3.604	n.d.	
		3.210	n.d.	
		3.183	3.181	0.999
		3.157	3.160	1.001
		3.116	3.110	0.998
		2.951	n.d.	
		2.509	2.519	1 004
		2.500	2.505	1.002
		*Carbonaceous Chondrite (Chamosite 13-29)**		
002	7.05	7.177	7 179	1.000
003,020	4.71	n.d.	4.687	
004	3.53	3.571	3.574	1.001
005	2.84	2.876	n d.	
200	2.70	2.685	n.d.	
202	2.52	2.530	2.531	1.000
204	2.15	2 164	2 166	1.001
206,240	1.778	n.d.	1.797	
060	1.558	1.563	1.569	1.004
		Carbonaceous Chert		
		9.209	9.215	1.001
		7.042	7.047	1.001
		4.718	4.720	1.000
		3.820	3.824	1.000
		3.675	3.678	1.001
		3.545	3 546	1.000
		3.323	3.323	1.000
		3.105	3.106	1.000
		3.011	3.013	1.000
		2.876	2.876	1.000
		2.855	2.855	1.000
		2.663	2.664	1.000
		2.533	2.532	1.000
		2.478	2.480	1.001
		2.397	2.397	1.000
		2.272	2.271	1.000
		2.187	2.187	1.000
		2.083	2.083	1.000
		2.011	2.011	1.000
		1.902	1.903	1.000
		1.866	1.866	1.000
		1.803	1.803	1.000
		1 784	1.785	1.000
		*Phyllosilicate (Montmorillonite 29-1498)**		
001	13.6	11.8	11.8	1.000
11-,02-	4.46	4.458	4.438	0.995
005	3.13	3.212	3 201	0 997
13-20-	2.56	2.559	2.556	0.999
		*Halite (5-628)**		
111	3.258	3.225	3.228	1.001
200	2.821	2.797	2.799	1.001
220	1 994	1.984	1.985	1.000
222	1 628	1.622	1.623	1.000

hkl, Miller indices; PDF, interplanar spacings (angstroms) from Mineral Powder Diffraction File [*JCPDS*, 1980]; Ctrl, measured interplanar spacings (angstroms) for control sample; Irrad, measured interplanar spacings (angstroms) for irradiated sample; n.d., not detected.

* *JCDPS* [1980] data card

\# Aragonite 041 and 202 peaks not resolved separately in control sample

The isotopic composition of Sm was also analyzed to verify that no thermalized neutrons were produced as a result of the irradiation. Basalt samples, unirradiated and irradiated at 3 x 10^7 rads, were analyzed. Both the $^{149}Sm/^{152}Sm$ and $^{150}Sm/^{152}Sm$ ratios were the same for the two splits, within $\pm 2\sigma$ (Table 3).

The thermal neutron cross sections for Nd isotopes are much smaller than those for Sm isotopes, so the lack of radiation effects on Sm implies that such effects are also negligible for Nd. Thus radiometric age determinations by the ^{147}Sm-^{143}Nd method should not be affected by gamma irradiation.

5.2 Effects of Radiation on Rocks and Minerals: Elemental Composition

5.2.1 Instrumental neutron activation analysis. Analytical results for control and irradiated basalt samples are presented in Table 4. Twenty-seven of 28 major, minor, and trace element concentrations were unchanged (within analytical error) following irradiations at 3 x 10^5, 3 x10^6, and 3 x10^7 rads. The single exception was Au (concentrations approximately 10 ng/g), with two higher and two lower values. The variation was at a level at least an order of magnitude smaller than any other INAA data and probably represented natural variation in the concentration of this trace element. In any case, the Au concentration did not vary directly with radiation dose.

5.2.2 Inductively coupled plasma emission spectrometry. Table 5 provides the analytical results for 17 elements in control and irradiated (3 x 10^7 rads) samples. For all samples, the major and minor element concentrations (>1000 ppm) fall within $\pm 3\sigma$ ($\pm 6\%$). Larger differences in the trace element concentrations are judged to be the result of poor counting statistics and statistical variability between splits.

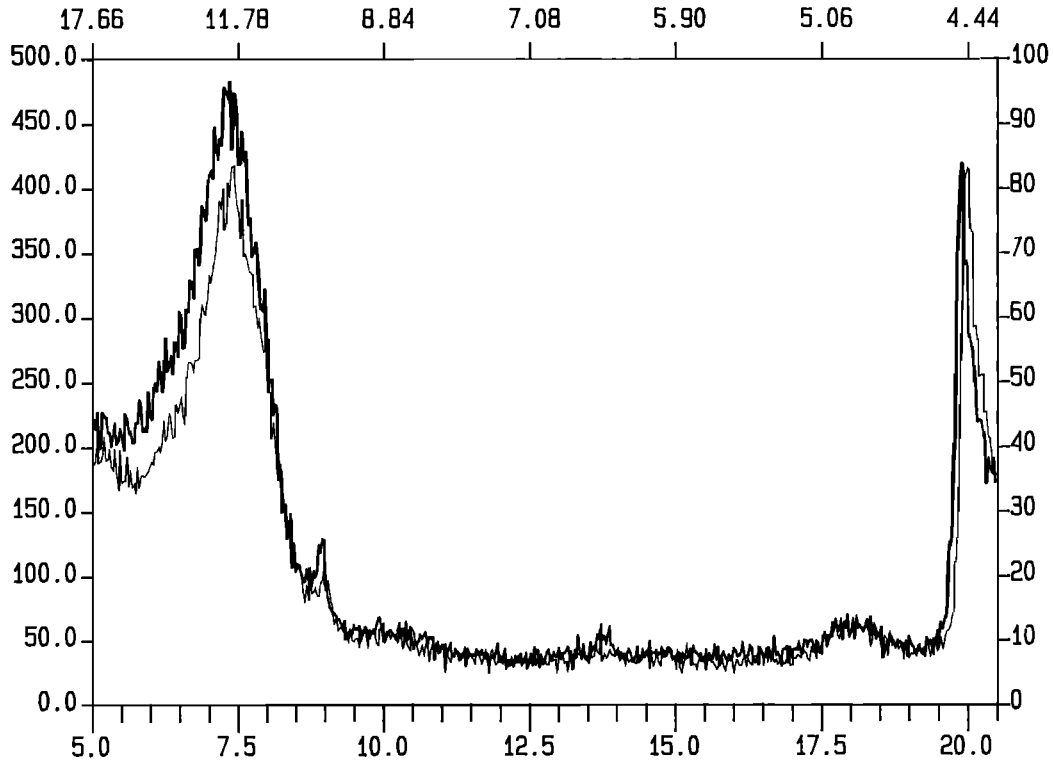

Figure 1. XRD patterns of unirradiated phyllosilicate (upper pattern) and phyllosilicate exposed to 3 x 10^7 rads; tallest peaks correspond to basal spacing (11.8 angstroms); 2θ range 5° to 20.5°.

5.3 Effects of Radiation on Rocks and Minerals: Crystal Structure, Surface Area, and Fluid Inclusions

5.3.1 X-ray diffraction. The XRD patterns of control and irradiated (3 x 10^7 rads) powders were essentially identical for all samples. For the dominant peaks, all interplanar spacings were unchanged to a precision of <0.5% (Table 6). The peak widths of control and irradiated samples were indistinguishable. The basal spacing of the phyllosilicate montmorillonite, which is extremely sensitive to temperature and degree of hydration, was not affected by irradiation (Figure 1). With the exceptions of the heterogeneous Mars soil simulant and carbonaceous chondrite samples, no peak was observed in a spectrum from an irradiated sample which was not present in the spectrum from the corresponding control, and vice versa. This observation indicates that no crystalline phases were formed or destroyed within the detection limits of the technique (approximately 5%). In particular, there was no evidence for significant dehydration of gypsum ($CaSO_4$ $2H_2O$) to anhydrite ($CaSO_4$; Figure 2).

5.3.2 Thermal emission (vibrational) spectroscopy. Figure 3 shows the spectra of four pyroxene splits. Diagnostic spectral features are unchanged in shape or position as a result of irradiation. The only variations among the spectra are differences in band depth, but there is no correlation between band depth and radiation dose. These depth variations probably result from particle size differences among the splits.

The gypsum spectra also show no changes in band positions but significant differences in band depth related to sample particle size. Variations in band depth do not correlate to amounts of radiation exposure.

The aragonite spectra are typical of very fine particulate samples and display differences in band depth similar to those observed in the pyroxene and gypsum. As in those cases, the variations between aragonite spectra most likely result from particle size differences between the splits. There are no differences in the locations or shapes of the features that would suggest any change in the fundamental vibrational character of the mineral as a result of exposure to radiation.

The Mars soil simulant exhibits weak absorption near 10 μm and stronger features at wavelengths longer than 15 μm. In these regions, extremely minor differences in band depth are present. Again, the absence of changes in position or shape of the features indicates that no change in the vibrational character of the mineral has occurred.

The halite sample (Figure 4) does show minor changes (increase in spectral contrast) in the 6 to 16 μm region of the spectrum. The emissivity maximum centered at 9 μm in the control sample is much less pronounced in the irradiated sample. Similarly, emission minima near 9.5 and 11.5 μm in the control sample are almost indiscernible in the irradiated sample. This reduction in contrast across the spectrum may be attributable to an overall finer grain size in the irradiated split or to changes in the vibrational nature of halite or its contaminant phases.

The optical properties of halite differ from the other minerals described here and thus may provide insight into the source of these variations in the spectrum. Because halite is highly ionic, the chemical bonds between Na and Cl do not produce independent vibrations observable in the thermal infrared, but the crystal lattice as a whole vibrates [*Simon*, 1966]. The result is a strong absorption feature in the emissivity spectrum which is significantly broader than the anion-related vibrational features of other minerals [*Lane and Christensen*, 1998]. As a result of the essentially featureless nature of the halite spectrum, features resulting from very minor contaminant minerals are particularly apparent and resemble the composite transmission spectrum of the impurities [*Eastes*, 1989]. In the emissivity spectrum,

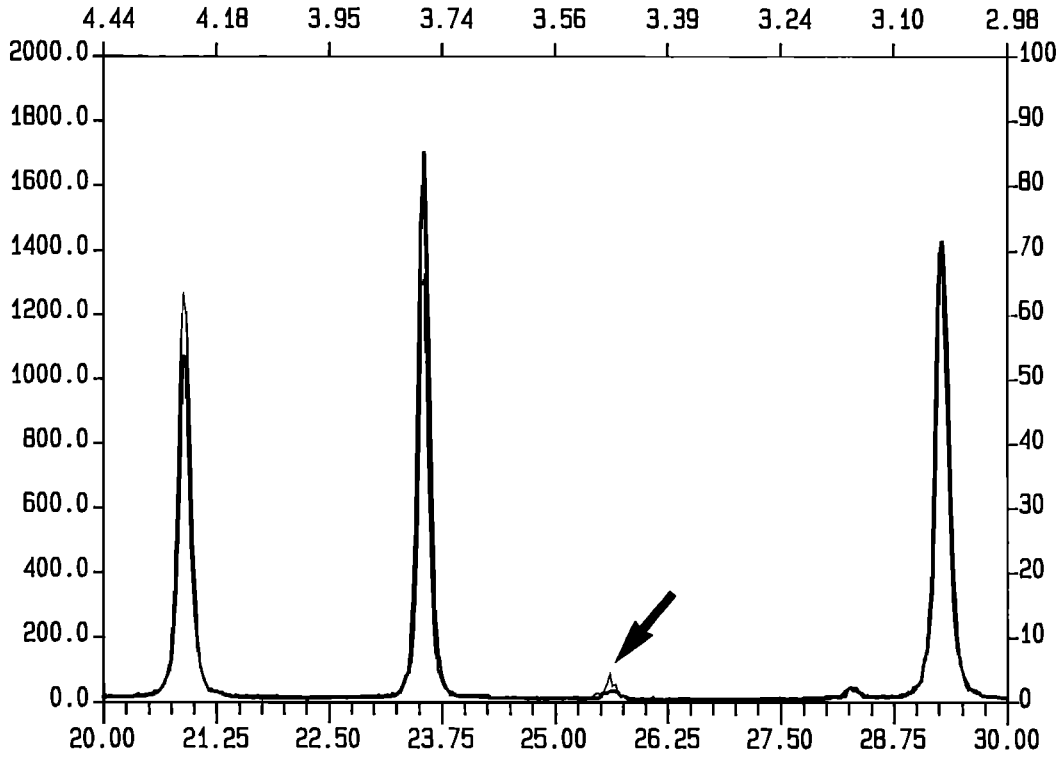

Figure 2. XRD patterns of unirradiated gypsum (upper tallest peak) and gypsum exposed to 3 x 10^7 rads; arrow denotes position of dominant anhydrite peak (3.498 angstroms); 2θ range 20° to 30°.

transmission features of the contaminant(s) in the halite appear as peaks.

The halite sample examined in this study is essentially pure NaCl, with minor contamination by clay, gypsum, polyhalite, and calcite (Table 1). These impurities may account for peaks in the shorter-wavelength (<12 μm) region of the spectrum (Figure 4). Mineral contaminants at the <1% level have been previously observed in the thermal emission spectra of halite [*Lane and Christensen*, 1998] and probably produce the spectral features in the halite samples in this study. If so, the observed changes in

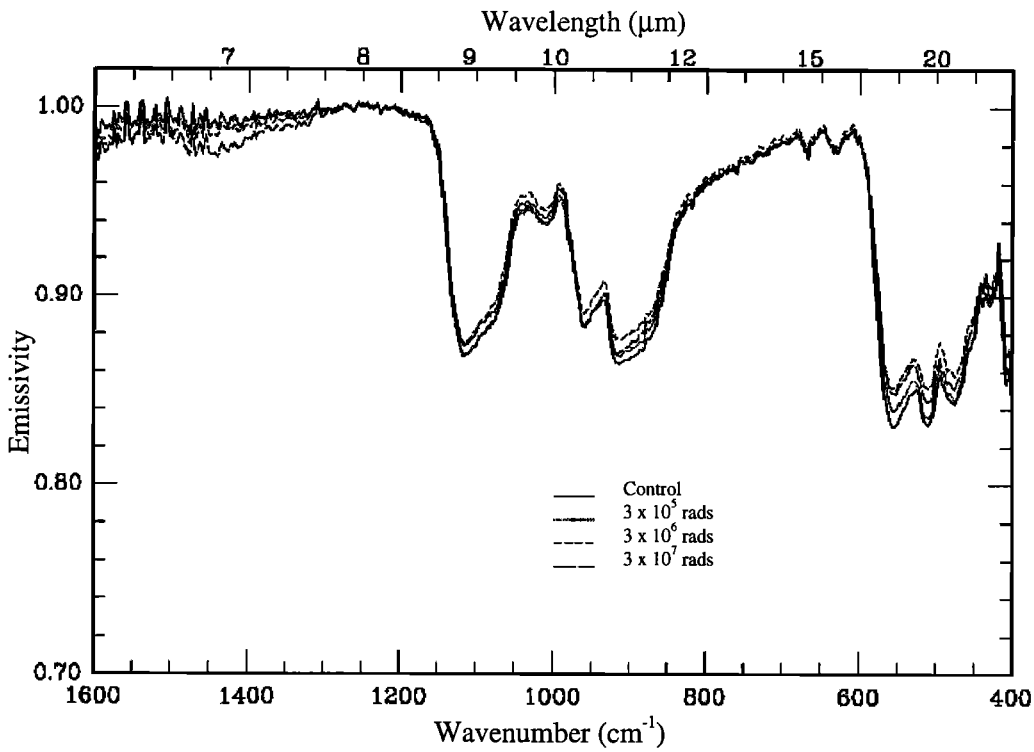

Figure 3. Thermal emission (vibrational) spectra of unirradiated and irradiated pyroxene splits.

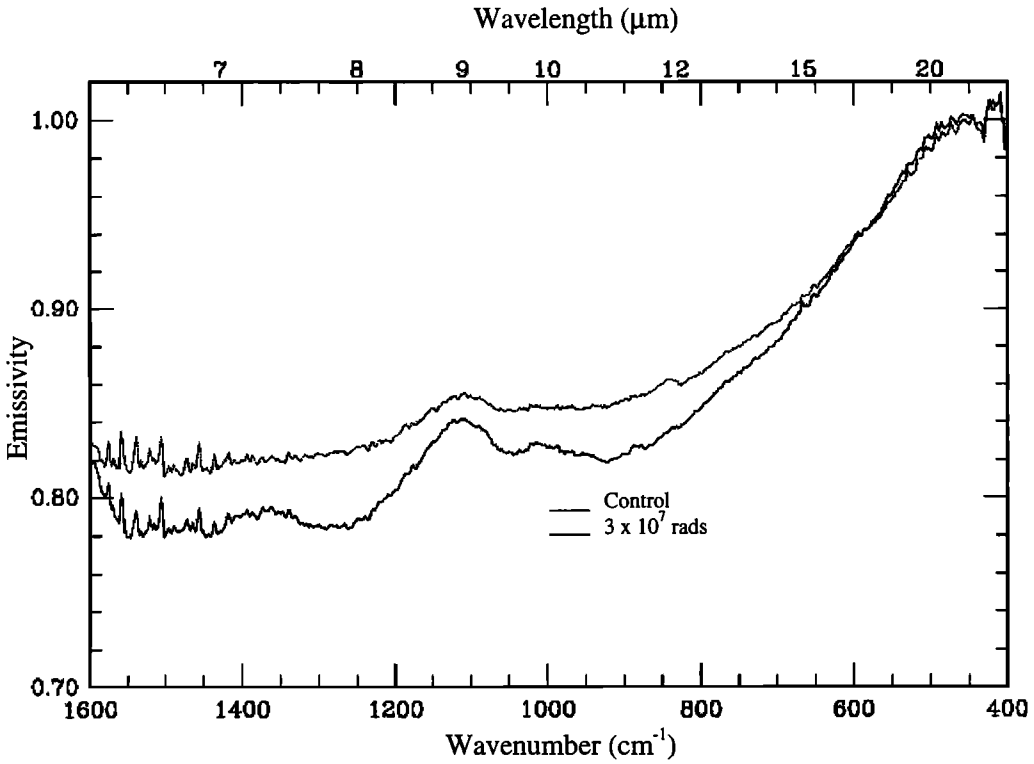

Figure 4. Thermal emission (vibrational) spectra of unirradiated and irradiated halite splits.

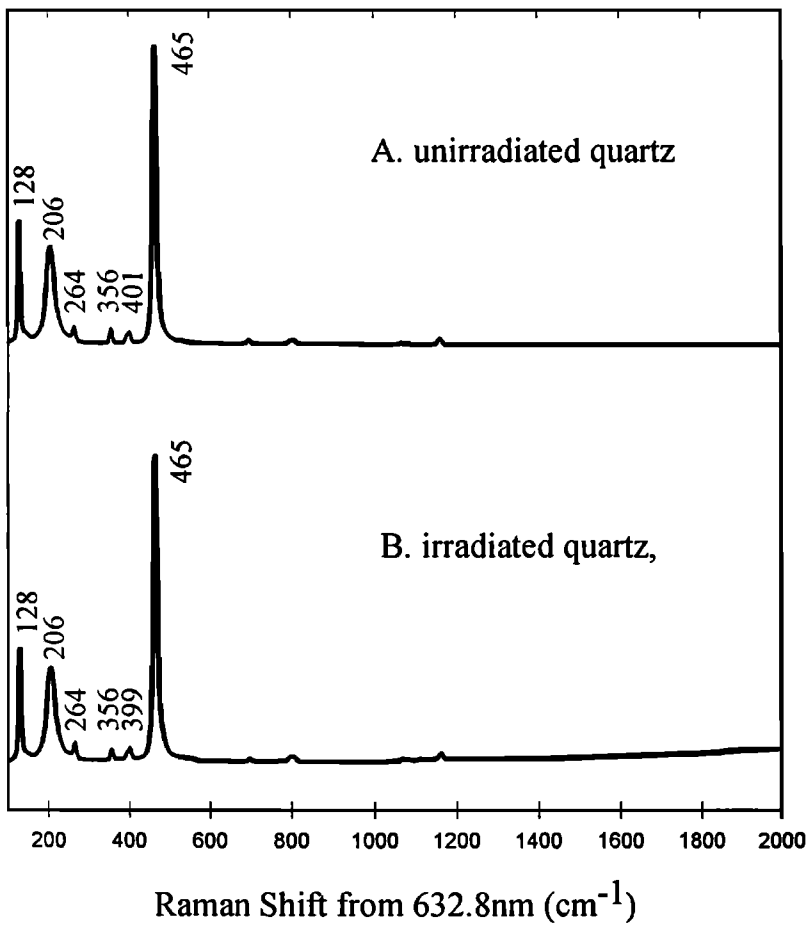

Figure 5. Raman spectra of quartz samples from the unirradiated split and the split exposed to 3 x 10^7 rads.

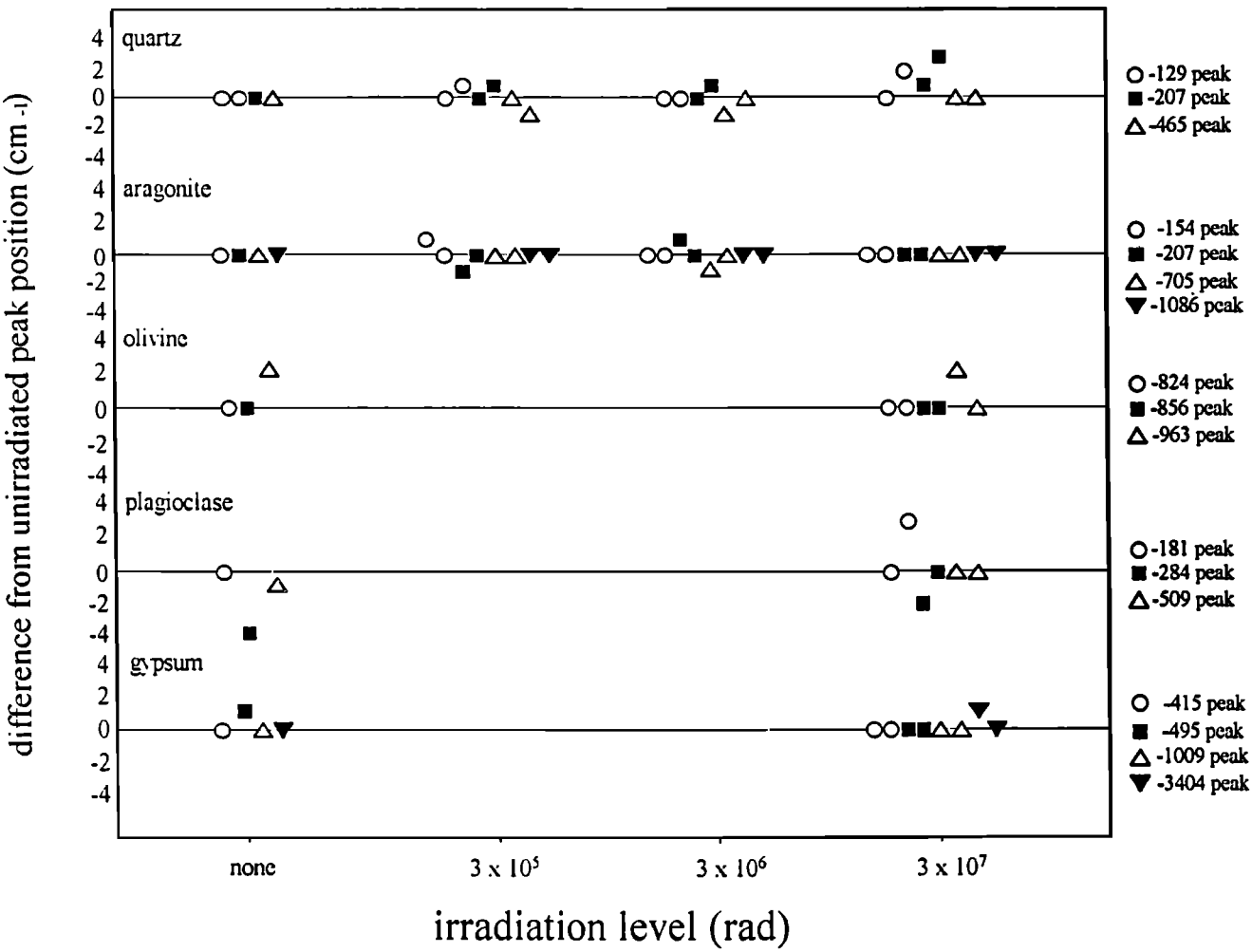

Figure 6. Position of the major Raman peaks as a function of radiation dose.

spectral features may represent changes in the contaminant minerals, not the halite itself. Alternatively, spectral changes may not result from irradiation but simply from the differing abundances of contaminants between splits of the halite sample. Without further analysis, it is difficult to determine which of these effects is producing the observed characteristics. However, these spectral variations are relatively minor overall and would not preclude the identification of halite in the case of an irradiated sample.

5.3.3 Raman Spectroscopy. The primary and essential capability of Raman spectroscopy is to obtain characteristic spectra so that the mineralogy of individual grains in a geologic sample can be identified. Variations in the shape of spectra, including the background, and in the shape, intensity, width, and position of specific Raman peaks must be considered. Crystallographic orientation can affect relative peak intensities, particularly for Raman features which are composed of two or more overlapping peaks. A minor peak shift can appear in such composite peaks when measuring two grains with different orientations. Multiple analyses of each sample split are made in order to distinguish potential effects of irradiation from those resulting from other sample factors.

In the present experiments, no significant changes in the peak intensities or positions of the irradiated splits relative to the unirradiated splits were observed. As an example, the essentially identical spectra of control and irradiated quartz are compared in Figure 5.

The Raman spectra show no correlation between variations in peak position and irradiation level for any of the major Raman peaks of any mineral sample set. Figure 6 compares the differences in major peak positions in the Raman spectra for control and irradiated grains. Differences in peak position in the spectra of two grains of the same unirradiated sample reflect heterogeneity in the sample or uncertainties related to the determination of peak positions. Figure 6 shows clearly that, although variations exist in our measurements of peak positions, they are not systematically related to irradiation levels.

One possible effect of gamma irradiation might be to alter the background fluorescence of the Raman spectra. Broad background fluorescence humps or peaks, commonly observed in Raman spectra, are mainly caused by emissions from electronic transitions in ions such as Mn^{2+}, Cr^{3+}, or Cu^{2+}. If the irradiation were to induce some change in the valence state of these ions or the properties of the crystal field surrounding them, the shape of the background and the central wavelength of the background fluorescence in their Raman spectra might vary [*Heymann*, 1988]. The quartz and aragonite samples showed significant variations in background fluorescence; however, these did not correlate with irradiation level and thus are attributable to the heterogeneity typically observed in geologic materials.

Another potential effect that might conceivably be associated with irradiation is variation in peak intensity. In metamict geologic materials, those whose structures have been degraded by alpha-decay events caused by naturally occurring radionuclides, a

Table 7. Effects of Gamma Radiation on Specific Surface Area of Mars Soil Simulant and Phyllosilicate

	Specific Surface Area, m^2/g			
Sample	Control	3×10^5 rads	3×10^6 rads	3×10^7 rads
Mars soil simulant	136 ± 5	144 ± 2	142 ± 3	not analyzed
Phyllosilicate	705 ± 7	693 ± 3	699 ± 2	703 ± 5

Mean of three measurements for each sample. Uncertainties ±1σ from the mean.

broadening of Raman peaks and a loss of intensity can occur as a result of progressive alteration of the mineral's molecular structure [*Wopenka et al.*, 1996]. At the tested gamma doses, no such spectral effects were observed. Radiation doses as high as 3×10^7 rads will not affect mineral identification and characterization using Raman spectroscopy.

5.3.4 Specific surface area. Results of the SSA measurements are presented in Table 7. Gamma radiation doses as high as 3×10^6 rads and 3×10^7 rads had little or no effect on the specific surface areas of Mars soil simulant and phyllosilicate samples, respectively. Multivariable regression analysis (gamma radiation dose and sample type as independent variables, n=17, R^2=0.99) demonstrated no statistically significant effect of the radiation on specific surface area. The constancy of specific surface area supports convincingly the conclusion that the radiation has not changed the subtle structure of the mineral(s) in the two samples studied.

5.3.5 Fluid inclusions. The major concern for fluid inclusions with respect to gamma irradiation of Martian samples is whether the irradiation process affects the homogenization temperature of the inclusions. The TH may be modified if the volume of the inclusion changes through a process referred to as stretching [*Bodnar and Bethke*, 1984] or if some fluid is lost from the inclusion by leakage along microfractures [*Bodnar et al.*, 1989; *Vityk and Bodnar*, 1998]. Conversely, if the TH remains constant, it is generally assumed that the inclusion has neither changed volume nor lost any of its contents. In order to test for possible stretching or leakage of the inclusions as a result of gamma irradiation, TH of the same inclusions measured before irradiation was measured after irradiation.

Note that 55 inclusions were analyzed before irradiation, but only 48 of these were analyzed after irradiation. This is because one of the quartz plates broke during shipment, and the crack intersected the area containing seven of the inclusions and destroyed them. The remaining 48 inclusions, however, were intact. The difference in homogenization temperature (TH after irradiation minus TH before irradiation) is shown in Figure 7. Homogenization temperatures of all the inclusions as measured both before and after irradiation agreed within ±0.4°C. In most fluid inclusion studies, the precision of successive TH measurements on a given fluid inclusion is reported to be ±1°C. The results (Figure 7) are well within this limit and show conclusively that the homogenization temperatures of fluid inclusions in quartz were not affected by a dose of 3×10^7 rads.

5.4 Effects of Radiation on Rocks and Minerals: Optical Properties and Thermoluminescence

5.4.1 Color. Single crystals of quartz, initially transparent and colorless, were strongly colored and darkened by irradiation (Figure 8). The degree of darkening increased with dose, most

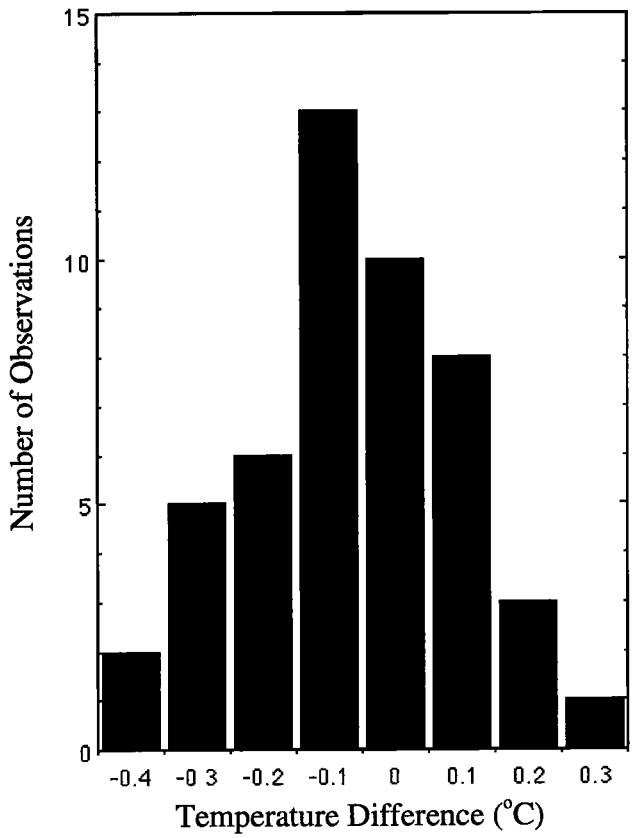

Figure 7. Differences in the measured homogenization temperatures (TH after minus TH before) of 48 fluid inclusions in quartz, as determined before and after irradiation at 3×10^7 rads.

apparently between 3×10^5 and 3×10^6 rads, with an overall brown to grey color. Crystals exposed to 3×10^7 and 1×10^8 rads were essentially opaque. Darkening was not uniform throughout the quartz crystals but was concentrated in bands parallel to the crystal faces (Figure 9). Electron microprobe analysis demonstrated that the dark bands correlated with Al_2O_3 concentrations of approximately 250 ppm, versus 100 ppm in the intervening light bands.

Halite crystals also darkened with increasing dose, with the most marked change between the 3×10^5 and 3×10^6 rad samples.

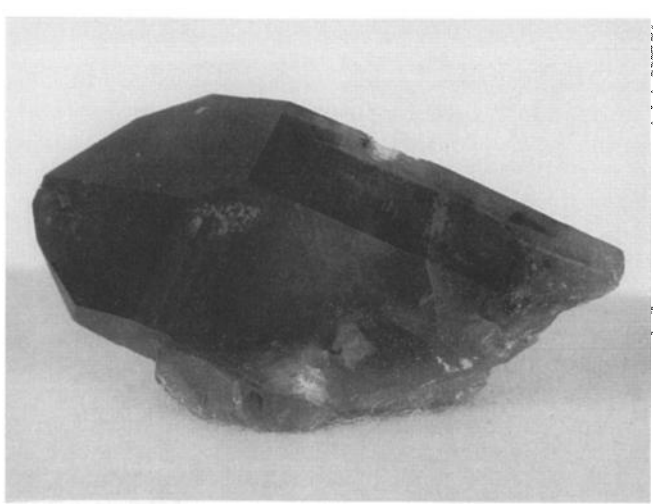

Figure 8. Quartz crystal darkened by exposure to 3×10^7 rads; crystal width 2.5 cm.

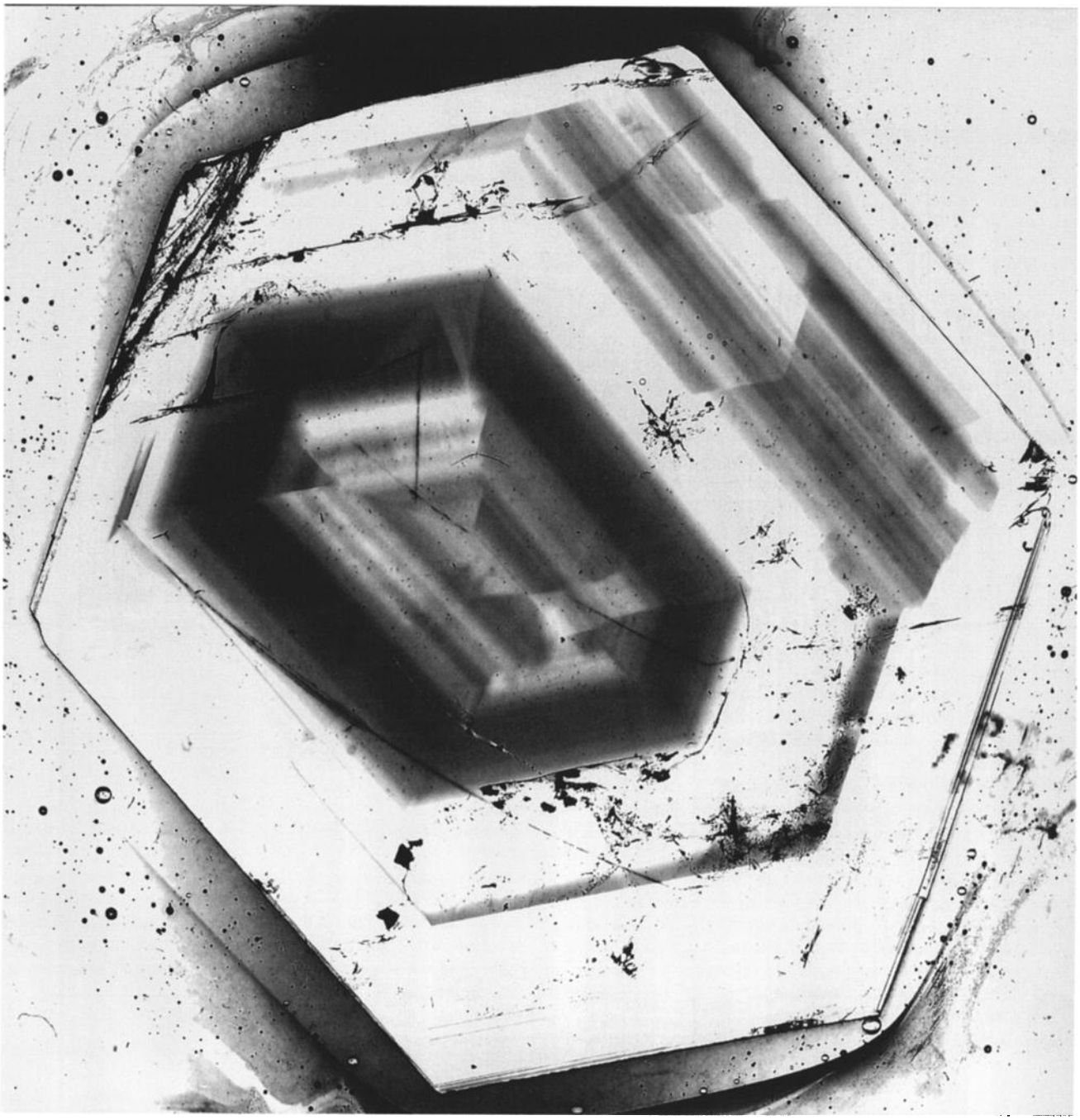

Figure 9. Cross section, perpendicular to C axis, of quartz crystal exposed to 3 x 10^7 rads; dark core and bands are due to radiation exposure; dark speckles are fluid inclusions; transmitted light image, crystal width 2.5 cm.

The dominant color was deep blue. Halite exposed to 1 x 10^8 rads was opaque.

The basalt powder irradiated at 3 x 10^7 and 1 x 10^8 rads also appeared visibly darker than the controls. Darkening was not observed in any other rock or mineral sample.

5.4.2 Visible and near-infrared reflectance spectroscopy. Diffuse reflectivity spectra (350 to 2100 nm) were obtained for the <0.1 mm size fraction of all rock and mineral samples, except for the phyllosilicate and Mars soil simulant, which were a fine powder and the <1 mm size fraction, respectively. In addition, a chip of unirradiated quartz was ground to a fine powder in an alumina mortar and pestle and analyzed to assess the contamination caused by grinding samples in tungsten carbide.

Reflectivity spectra for quartz are shown in Figure 10. Note that the three control samples (labeled "0 rad") have very different levels of reflectivity. At 1000 nm the reflectivity of the sample ground with an alumina mortar and pestle is approximately 0.97 and that for the two samples ground in the tungsten carbide shatter box are around 0.70 and 0.62. Because quartz is a hard mineral, it is difficult to crush and grind without contamination. Thus the sample ground in white (and hard) alumina has a high reflectivity, and the two samples ground in grey tungsten carbide are significantly less reflective. Presumably, the differences in reflectivity for the two control samples ground in tungsten carbide result from different grinding times. The effect of grinder material on quartz spectra is

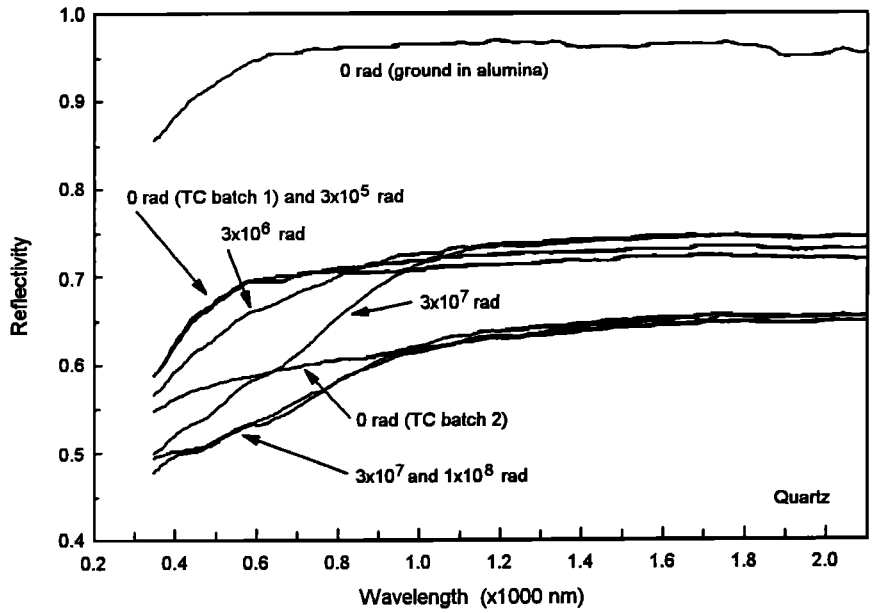

Figure 10. Diffuse reflectivity spectra (20°C) for control and irradiated samples of quartz. The two control (unirradiated) samples ground in tungsten carbide (TC batch) have lower reflectivities than the sample ground in alumina because of tungsten carbide contamination. The irradiation-induced decrease in reflectivity between approximately 400 and 1000 nm results from the formation of color centers (Al trapped-hole centers).

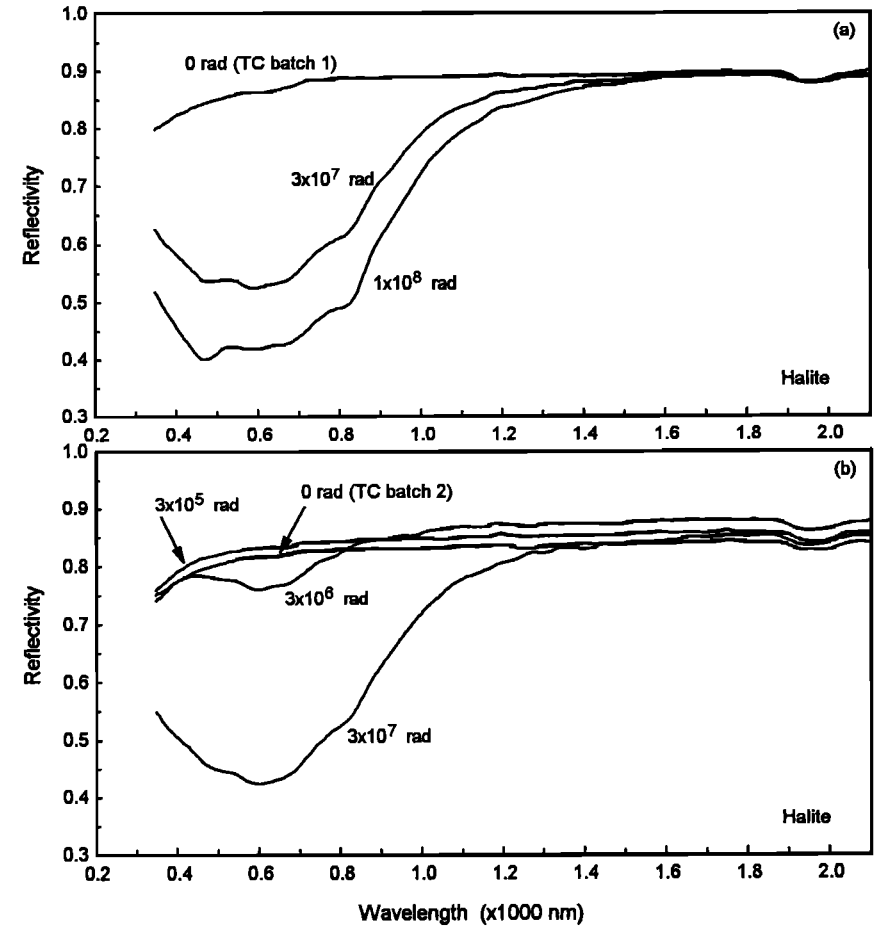

Figure 11. Diffuse reflectivity spectra (20°C) for two batches (Figures 11a and 11b) of control and irradiated samples of halite, both ground in tungsten carbide. The absorption centered near 600 nm in the irradiated samples results from formation of color centers (electrons associated with anion vacancies).

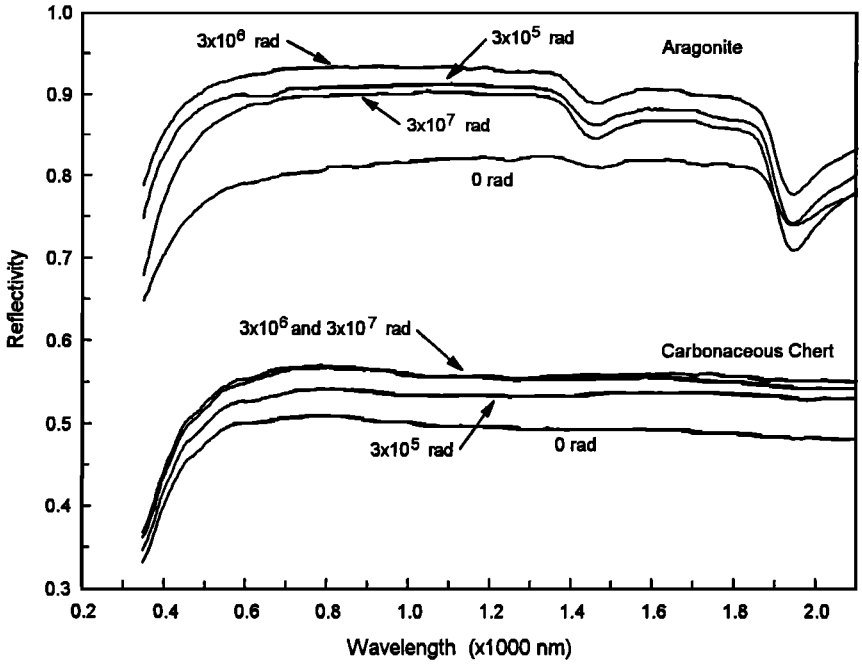

Figure 12. Diffuse reflectivity spectra (20°C) for aragonite and carbonaceous chert. Irradiation results in a uniform increase in reflectivity over the entire spectral range. Formation of color centers similar to those in quartz and halite was not observed.

discussed by *Hunt and Salisbury* [1970], who also point out that weak spectral features can be obscured by this contamination. In any case, the contamination means that spectral comparisons must be made on control and irradiated samples that came from the same batch of powdered material.

Figure 10 shows two sets of control and irradiated quartz powders. In both cases, ^{60}Co irradiation results in a regular decrease in reflectivity between approximately 350 and 1000 nm with increasing dose. This is a well-documented phenomenon that results from the formation of color centers. The irradiated sample matches the color of smoky quartz, which has color centers due to aluminum trapped-holes associated with an Al^{3+} impurity [*Cohen*, 1985]. The correlation of darkening with increased aluminum concentration was noted in irradiated quartz crystals (above). The threshold level of 3 x 10^6 rads is an upper limit because of tungsten carbide contamination.

As expected from prior work [*Pederson*, 1985], the spectral properties of halite are strongly altered by irradiation (Figure 11). The blue coloration results from formation of F centers (electrons associated with anion vacancies) and possibly other color centers [*Kittel*, 1967]. The threshold level is between 3 x 10^5 and 3 x 10^6 rads.

The irradiated carbonate-bearing samples (aragonite and carbonaceous chert) are uniformly brighter than the control samples (Figure 12), even at the lowest dose level (3 x 10^5 rads). The variation is systematic for carbonaceous chert but not for aragonite where the 3 x 10^7 rad sample is generally more reflective than the control samples but less reflective than the 3 x 10^5 and 3 x 10^6 rad samples. Additional work is needed to understand the uniform brightening of these carbonate-bearing materials.

Figure 13 shows reflectivity spectra for pyroxene (diopside), olivine, plagioclase, and basalt. No radiation-induced changes were observed for diopside and olivine, although we did not have a control sample for olivine. Except for a small decrease in reflectivity at wavelengths below approximately 430 nm, we did not observe any systematic effects associated with irradiation. The basalt powders behaved quite differently. As noted above, the samples irradiated at 3 x 10^7 and 1 x 10^8 rads appeared visibly darker than the controls. This observation was confirmed by comparing the traces for the control sample to the first-scan trace for 1 x 10^8 rads (Figure 13). After removing the irradiated sample from the spectrometer and returning it to its storage vial, we observed that it and the control were nearly the same shade of grey. A second scan (Figure 13) confirmed this observation. We do not currently understand the mechanism for uniform darkening or the reason the effect seemed to disappear after measurement and removal of samples from the spectrometer.

Reflectivity spectra for control and irradiated samples of gypsum, phyllosilicate, Mars soil simulant, and carbonaceous chondrite are shown in Figure 14. We see no systematic spectral variations that can be attributed to ^{60}Co irradiation. There are significant differences in the intensities of the band near 1900 nm (associated with H_2O) for phyllosilicate samples (Figure 14b), but the differences are not systematic. The reflectivity of the control samples is lower than that of the irradiated samples in the upper traces and vice versa in the lower traces. Because there was no control on the humidity before, during or after irradiation, we are hesitant to draw any conclusions regarding bands associated with H_2O and OH. It is appropriate to conclude, however, that new bands were not introduced in our irradiation experiments.

5.4.3 Thermoluminescence. Results from the induced TL analysis of quartz and plagioclase are presented in Table 8. The sensitivity of each irradiated sample is normalized to that of the respective control sample, so that values greater than unity indicate a change resulting from irradiation. The temperature of maximum emission (TL Peak Temp.) and width of the peak (TL Peak Width) are related to the structural state of the phosphor in the case of plagioclase [*Guimon et al.*, 1985] and reflect the energy depth distribution of the electron traps. Changes in TL peak shapes reflect changes in the trap population.

The present study demonstrates significant changes to the TL

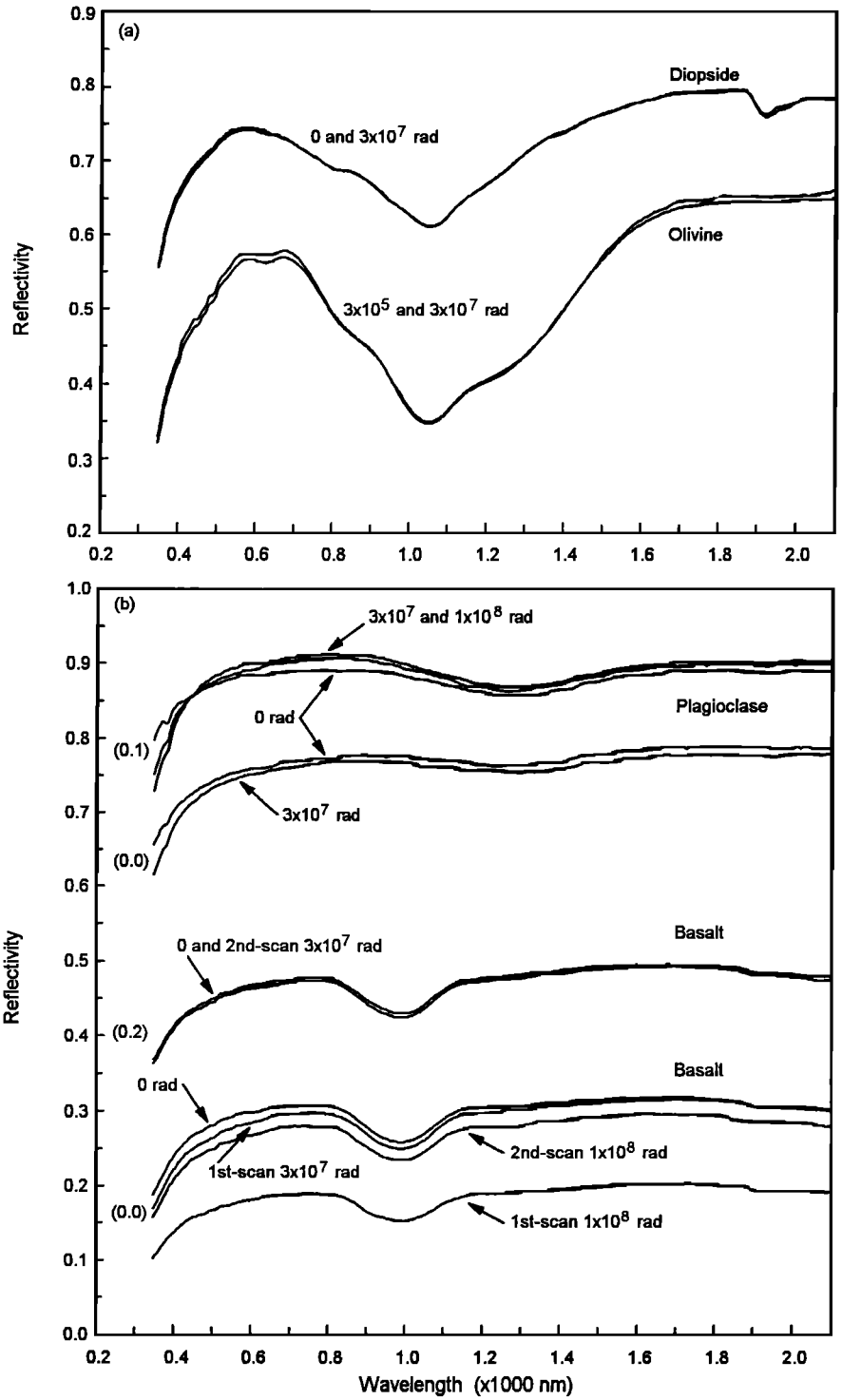

Figure 13. Diffuse reflectivity spectra (20°C) for (a) pyroxene (diopside) and olivine and (b) plagioclase and basalt. Minimal to no variation was observed for diopside, olivine, and plagioclase. The basalt uniformly darkened, but returned to previous levels of reflectivity on scans repeated at later times. Formation of color centers similar to those in quartz and halite was not observed.

properties of quartz with increasing gamma dose. The control sample produces a typical quartz glow curve with a very narrow peak at low temperature (108°C) and very little high-temperature emission (Figure 15a). In contrast, the sample exposed to 3 x 10^7 rads retains the low-temperature peak (with a modest increase in sensitivity relative to the control sample), whereas the high-temperature (400°C) emission increases by a factor of over 5700 (Table 8, Figure 15b). The glow curve from the sample irradiated at 1 x 10^8 rads is essentially indistinguishable from that of the 3 x 10^7 rad sample.

The TL properties of the plagioclase sample also show changes with increasing gamma dose, although the changes are

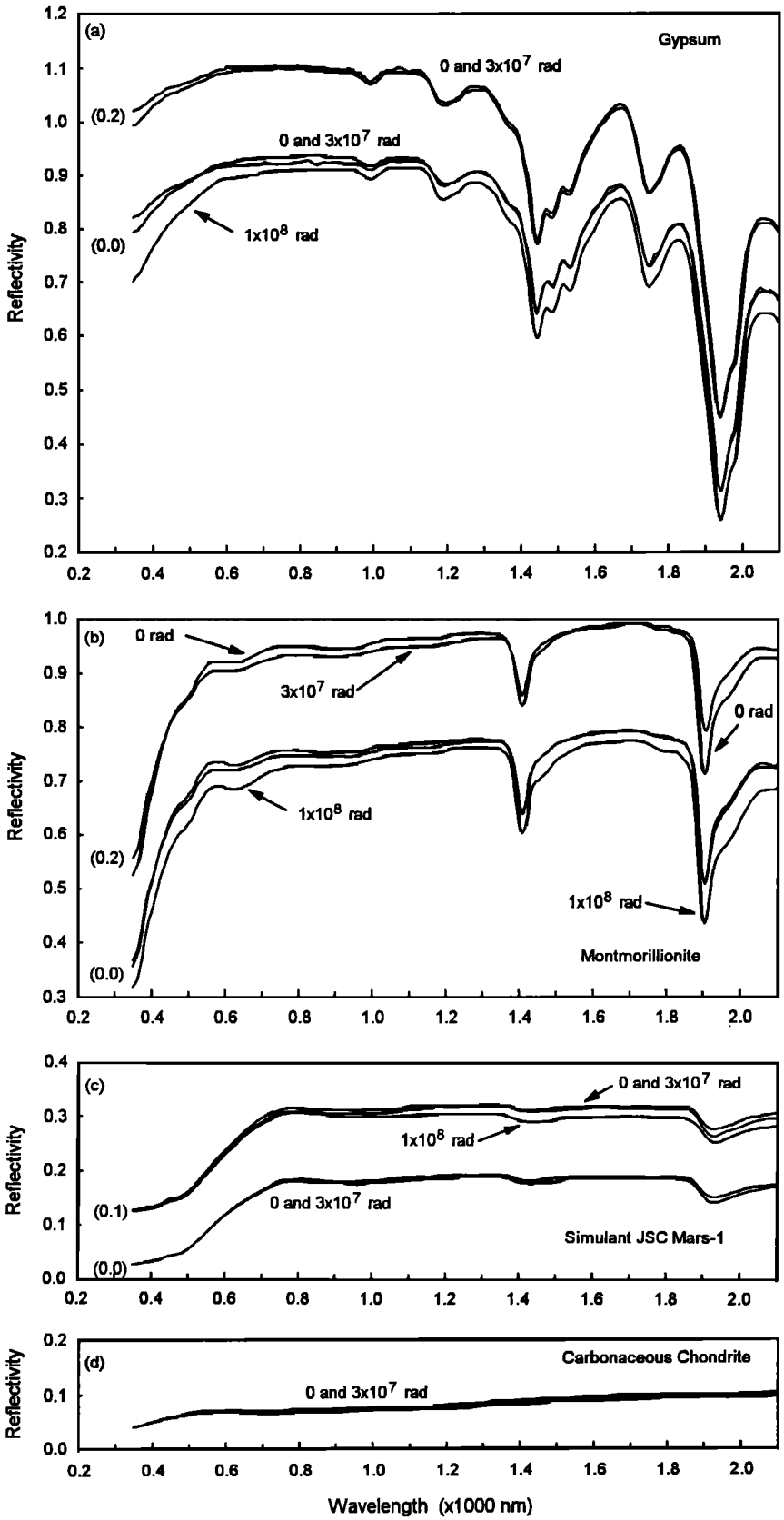

Figure 14. Diffuse reflectivity spectra (20°C) for (a) gypsum, (b) phyllosilicate (montmorillonite), (c) Martian soil simulant JSC Mars-1, and (d) carbonaceous chondrite. No spectral changes were systematically correlated with radiation dose. Formation of color centers similar to those in quartz and halite was not observed.

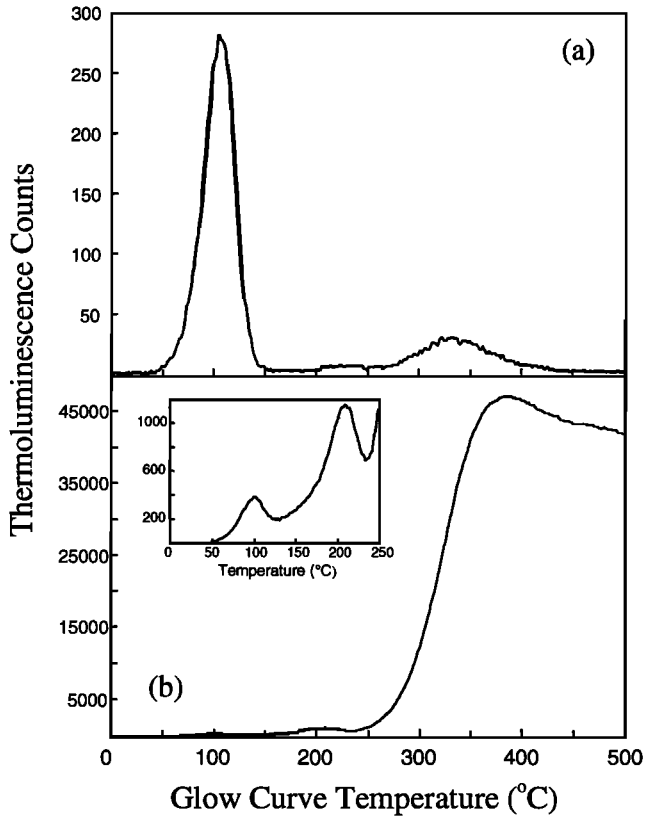

Figure 15. Induced TL glow curves for (a) unirradiated quartz and (b) quartz exposed to 3 x 10^7 rads of gamma irradiation. Note the different scales on the y axis. The inset of Figure 15b shows that the low-temperature peak seen in the unsterilized sample is still present after irradiation but that it is overwhelmed by the high-temperature emission. A 220°C peak barely visible in the control sample is much more pronounced in the irradiated material.

much less dramatic than those displayed by quartz. Neither the peak temperature nor the peak width is affected by irradiation, but the sensitivity increases by approximately 30% over that of the control sample (Table 8). These changes occur only after a dose of 3 x 10^7 rads. Lesser doses cause no detectable change in TL properties. As in the case of the quartz sample, further changes do not seem to take place after exposure to 1 x 10^8 rads. Only quartz and plagioclase have their TL properties measurably affected by irradiation, although the induced TL signals of the basalt, Mars soil simulant, and carbonaceous chondrite samples may be below detection limits.

6. Discussion

6.1 Dose-Dependent Effects of Gamma Radiation on Rocks and Minerals

These experiments demonstrate that ^{60}Co gamma photons in doses as high as 3 x 10^7 rads have no detectable effects on isotopic or chemical signatures. The results are in accord with decades of research which show that photon energies significantly higher than 1.33 MeV are required to induce nuclear transitions. Thus, if ^{60}Co gamma irradiation is used for Mars sample sterilization, isotopic and chemical data will be unaffected regardless of the dose.

The experiments also show no detectable effects of 3 x 10^7 rads on crystallographic or physical properties. The crystal structures, thermal infrared spectra, and Raman spectra of a range of samples are not altered, nor are the surface areas of Mars soil simulant and phyllosilicate nor the fluid inclusions in quartz. The lack of detectable effects may be due to insufficiently energetic gamma photons or insufficient absorbed doses. Additional research will be required to identify these thresholds.

Gamma radiation did induce significant changes in the optical and thermoluminescence properties of some samples. These properties relate to well-documented interactions of gamma rays with certain sensitive minerals. The changes did prove to be dose-dependent in the range 3 x 10^5 to 1 x 10^8 rads.

Table 8. Effects of Gamma Radiation on Thermoluminescence Properties of Quartz and Plagioclase

		Low Temperature TL			High Temperature TL	
Sample	Gamma dose, rads	TL Sensitivity	TL Peak Temp., °C	TL Peak Width, °C	TL Sensitivity	TL Peak Temp., °C
Quartz	Control	1.0	108 ± 5	34 ± 5	1.0	400
	3 x 10^7	1.53 ± 0.18	104 ± 7		5733 ± 420	400
	1 x 10^8	1.15 ± 0.15	104 ± 5		5867 ± 527	400
Plagioclase	Control	1.0	144 ± 7	111 ± 7		
	3 x 10^5	0.92 ± 0.11	144 ± 8	111 ± 6		
	3 x 10^6	1.00 ± 0.12	145 ± 6	110 ± 9		
	3 x 10^7	1.33 ± 0.14	144 ± 7	108 ± 5		
	1 x 10^8	1.33 ± 0.14	144 ± 5	113 ± 8		

Uncertainties ±1σ from the mean.

6.2 Implications for Mars Sample Return

Planetary protection policy for a Mars sample return mission is still evolving. The recent report of a NASA advisory panel [*NASA*, 1999], concluded "Early distribution of a subset of sterilized samples is an essential element in both scientific analysis of the samples and in assessing their potential for harm." The current study has implications which are directly relevant to this conclusion.

A sample handling and analysis strategy based on early distribution implies sterilization before any Martian life forms are identified or characterized. The sterilization method should therefore be lethal for all known life, with an additional measure of conservatism to account for possible adaptations of unknown Martian organisms. In the case of gamma radiation, sterilizing doses for most terrestrial bacteria and viruses are below 3×10^6 rads. However, some bacteria in desiccated or frozen conditions, similar to the Martian surface environment, tolerate significantly higher radiation doses. Active research is under way to establish the mechanisms for these increases in radiation tolerance and the maximum sterilizing doses for terrestrial organisms under a range of physical conditions. The maximum gamma dose for most of our experiments, 3×10^7 rads, may not prove to be lethal in all cases.

If conservative sterilization of Martian samples requires a higher gamma dose, much of the samples' value for geochemical research would still be preserved. Optical and thermoluminescence data from some minerals would certainly be altered, and some crystallographic and physical properties might be affected. Higher radiation doses would not, however, affect key measurements of chemical composition, isotope ratio, or radiometric age.

7. Conclusions

Martian analog rocks and minerals subjected to gamma doses as high as 3×10^7 rads showed no detectable changes in nuclear or mineralogical properties. Irradiation did not induce measurable radioactivity in rock and mineral samples. The activation of ^{117}Sn to ^{117m}Sn, a very sensitive test for induced radioactivity, could not be detected. No changes were produced in the ratios of Sr and Sm isotopes of basalt exposed to 3×10^7 rads. By inference, radiometric sample ages derived from these isotope ratios would also remain unchanged. Major, minor, and trace element abundances in rocks and minerals showed no detectable change as a result of irradiation. No changes were detected in the crystal structure of any sample as measured by lattice spacing and peak widths in powder XRD. No XRD peaks were removed nor added as a result of irradiation, indicating no bulk transformation of crystalline structures. No evidence of dehydration could be detected. Thermal emission and Raman spectroscopy showed no changes ascribable to irradiation. Specific surface areas of Mars soil simulant and a phyllosilicate were unchanged. Homogenization temperatures of fluid inclusions in quartz were not affected by irradiation.

Gamma irradiation in doses as high as 1×10^8 rads did cause changes in the optical properties and thermoluminescence of selected minerals. Quartz and halite, initially clear and colorless, steadily darkened under increasing gamma doses. Reflectance spectra confirmed the darkening of quartz and halite, as well as the brightening of aragonite and chert, with increasing radiation dose. No optical changes were detectable in any other sample. The thermoluminescence of quartz and plagioclase were markedly altered by irradiation.

In summary, gamma doses of 10^7 to 10^8 rads are lethal to a wide range of terrestrial microorganisms, even within a geologic matrix. Such doses to rocks and minerals do not induce radioactivity and have little or no effect on elemental or isotopic compositions or crystal structure. Changes are induced in the optical properties and thermoluminescence of certain sensitive minerals. On balance, if samples returned from Mars require biological sterilization, gamma irradiation provides a feasible option.

Acknowledgments. The authors acknowledge Craig Schwandt, David Mittlefehldt, Young Reese, Chi-Yu Shih, Henry Weismann, and Vincent Yang of Lockheed Martin; Joan Abramowitz at the University of Houston – Downtown; and Eric Grunwald, Adila Jamil, and Lauren Vigliotti of Boston University for valuable laboratory assistance. Thoughtful reviews by Jaclyn Allen, Michael Daly, and an anonymous referee improved the manuscript. Portions of this work were funded by the JSC Earth Science and Solar System Exploration Division (C.C.A.) and by the NASA Cosmochemistry program under grants NAG5-8343 (R.J.B.), NAG5-4642 to L. Haskin (B.L.J., K.K., A.W.), and RTOP 344-31-20-24 (R.V.M.). Additional support was provided by NASA Montana State University/TechLink contract 291558 under a Space Act Agreement with JSC (F.G.A., J.C.). Acquisition and initial maintenance of the ICP-ES facility at Boston University was supported by National Science Foundation EAR-9724282. We sincerely thank the institutions of all coauthors for support in kind.

References

Allen, C. C., and S. A. Rawson, Effects of irradiation and dry heating on bentonite: A transmission electron microscopy and x-ray diffraction study, in *Microbeam Analysis - 1986*, edited by A. D. Romig Jr. and W. F. Chambers, pp. 135-137, San Francisco Press, San Francisco, Calif., 1986.

Allen, C. C., K M. Jager, R. V. Morris, D. J. Lindstrom, M. M. Lindstrom, and J. P. Lockwood, Martian soil simulant available for scientific, educational study, *EOS Trans. AGU, 79*, 405-409, 1998.

American Society for Testing and Materials (ASTM), Standard practice for using the Fricke reference standard dosimetry system, *Standard E1026-95*, West Conshohocken, Pa., 1997.

Basaltic Volcanism Study Project (BVSP), *Basaltic Volcanism of the Terrestrial Planets*, Pergamon, Tarrytown, N. Y., 1981

Battista, J. R., DNA repair in *Deinococcus radiodurans*, in *DNA Repair in Prokaryotes and Lower Eukaryotes*, edited by J. A. Nickoloff and M. Hoekstra, pp. 287-303, Humana Press, Totowa, N. J., 1997a.

Battista, J. R., Against all odds: The survival strategies of *Deinococcus radiodurans*, *Annu. Rev. Microbiol., 51*, 203-224, 1997b.

Bodnar, R. J., and P.M. Bethke, Systematics of stretching of fluid inclusions, I, Fluorite and sphalerite at 1 atmosphere confining pressure, *Econ Geol., 79*, 141-161, 1984.

Bodnar, R. J., P. R. Binns, and D. L. Hall, Synthetic fluid inclusions, VI, Quantitative evaluation of the decrepitation behavior of fluid inclusions in quartz at one atmosphere confining pressure, *J. Metamorphic Geol., 7*, 229-242, 1989.

Bogard, D. D., M. B. Duke, E. K. Gibson, J. W. Minear, L E. Nyquist, and W. C. Phinney, Considerations of sample return and the exploration strategy for Mars, *NASA Tech. Memo., 58213*, 1979.

Carrigan, W. J., and E. M. Cameron, Petrological and stable isotope studies of carbonate and sulfide minerals from the Gunflint Formation, Ontario: Evidence for the origin of early Proterozoic iron-formation, *Precambrian Res., 52*, 347-380, 1991.

Carroll, J. J., et al., Photoexcitation of nuclear isomers by (γ,γ') reactions, *Phys. Rev. C , 43*, 1238-1247, 1991.

Carter, D. L., M. D. Heilman, and C. L. Gonzalez, Ethylene glycol monoethyl ether for determining surface area of silicate minerals, *Soil Sci., 100*, 356-360, 1965.

Chafetz, H. S., and J. R. Lawrence, Stable isotopic variability within modern travertines, *Geogr. Phys. Quatrinaire, 48*, 257-273, 1994.

Christensen, P. R., and S. T. Harrison, Thermal infrared emission spectroscopy of natural surfaces: Application to desert varnish coatings on rocks, *J. Geophys. Res., 98*, 19,819-19,834, 1993.

Clark, B. C., Surviving the limits to life at the surface of Mars, *J. Geophys. Res., 103*, 28,545-28,555, 1998.

Cohen, A. J , Amethyst color in quartz, the result of radiation protection involving iron, *Am. Mineral., 70.* 1180-1185, 1985.

Daly, M. J., L. Ouyang, and P. Fuchs, In vivo damage and recA-dependent repair of plasmid and chromosomal DNA in the radiation-resistant bacterium *Deinoccus radiodurans, J. Bacteriol., 176*, 3508-3517, 1994.

DeVincenzi, D. L., M. S. Race, and H. P. Klein, Planetary protection, sample return missions and Mars exploration: History, status, and future needs, *J. Geophys. Res., 103*, 28,577-28,585, 1998.

Eastes, J W., Spectral properties of halite-rich mineral mixtures: Implications for middle infrared remote sensing of highly saline environments, *Remote Sens. Environ., 27*, 289-304, 1989.

Elliott, L. H , J. B. McCormick, and K M. Johnson, Inactivation of Lassa, Marburg, and Ebola viruses by gamma irradiation, *J. Clinical Microbiol , 16*, 704-708, 1982.

Friedlander, G., J. W. Kennedy, and J. M. Miller, *Nuclear and Radiochemistry*, John Wiley, New York, 1964.

Gooding, J. L., Scientific guidelines for preservation of samples collected from Mars, *NASA Tech. Memo., 4184*, 1990.

Guimon, R. K., B. D. Keck, K. S. Weeks, J. M. DeHart, and D. W. Sears, Chemical and physical studies of type 3 chondrites, IV, Annealing studies of a type 3.4 ordinary chondrite and the metamorphic history of meteorites, *Geochim. Cosmochim. Acta, 49*, 1515-1524, 1985.

Heymann, D., Luminescence of experimentally shocked plagioclase feldspar (abstract), *Lunar Planet. Sci., XIX*, 489-490, 1988.

Hochstein, L. I., K. A. Kvenvolden, and D. E. Philpott, *The Effect of Sterilization on Biological, Organic Chemical and Morphological Information in Natural Samples*, NASA Planet. Biol. Program Off., Ames Res. Cen., Moffett Field, Calif., 1974.

Hunt, G. R., and J. W. Salisbury, Visible and near-infrared spectra of minerals and rocks, I, Silicate minerals, *Mod. Geol., 1*, 283-300, 1970.

JCPDS, *Mineral Powder Diffraction File, Data Book*, JCPDS Int. Cent. for Diffraction Data, Swarthmore, Pa., 1980.

Jockwer, N., and J. Monig, Laboratory investigation into the radiolytic gas generation from rock salt: A study related to the disposal of high level radioactive waste, in *Scientific Basis for Nuclear Waste Management*, edited by W. Lutze, pp. 913-919, Mater. Res. Soc., Pittsburgh, Pa., 1989.

Kantro, D. L., S. Brunauer, and L. E. Copeland, BET surface areas – Methods and interpretation, in *The Solid-Gas Interface*, edited by E. A. Flood, vol. 1, Marcel Dekker, New York, 1967.

Kittel, C. *Introduction to Solid State Physics*, John Wiley, New York, 1967.

Klein, H. P., The search for life on Mars: What we learned from Viking, *J. Geophys. Res., 103*, 28,462-28,466, 1998.

Krumhansl, J. L., Observations regarding the stability of bentonite backfill in a high-level waste (HLW) repository in rock salt, *Rep. SAND83-1293*, Sandia Natl. Lab., Albuquerque, N. M., 1986.

Lane, M. D., and P. R. Christensen, Thermal infrared emission spectroscopy of salt minerals predicted for Mars, *Icarus, 135*, 528-536, 1998.

Lange, C. C., L. P. Wackett, K. W. Minton, and M. J. Daly, Engineering a recombinant *Deinococcus radiodurans* for organopollutant degradation in radioactive mixed waste environments, *Nature (Biotech.), 16*, 929, 1998.

Ledney, G. D., G. B. Knudson, R. A. Harding, R. C. Bhatt, E. E. Kearsley, and J. A. Zmuba, Neutron and γ-ray radiation killing of *Bacillus* species spores: dosimetry, quantitation, and validation techniques, *Tech. Rep. 96-1*, Armed Forces Radiobiol. Res. Inst., Bethesda, Md., 1996.

Lindstrom D. J., and R. L. Korotev, TEABAGS: Computer programs for instrumental neutron activation analysis, *J. Radioanal. Chem., 70*, 439-458, 1982.

Lone, M. A., Induced radioactivity from industrial radiation processing, *Nucl. Instrum. Methods Phys. Res., A299*, 656-660, 1990.

MacPherson, G., *Antarct. Meteorite Newsl., 8(1)*, 16, 1985.

Mattimore, V., and Battista, J. R., Radioresistance of *Deinococcus radiodurans*: Functions necessary to survive ionizing radiation are also necessary to survive prolonged desiccation, *J. Bacteriol., 178*, 633-637, 1995.

McKeever, S. W., and D. W. Sears, Meteorites and thermoluminescence, *Meteoritics, 14*, 29-41, 1979.

Mittlefehldt, D. W., and M. M. Lindstrom, Geochemistry and petrology of a suite of ten Yamato HED meteorites, *Proc. NIPR Symp. Antarct. Meteorites, 6*, 268-292, 1993.

Moseley, B. E. B., Radiation damage and its repair in non-sporulating bacteria, in *The Revival of Injured Microbes*, edited by M. H. E. Andrews and A. D. Russell, pp. 149-170, Academic, San Diego, Calif., 1984.

Murray, R. W., and M. Leinen, Scavenged excess Al and its relationship to bulk Ti in biogenic sediment from the central equatorial Pacific Ocean, *Geochim. Cosmochim. Acta, 60*, 3869-3878, 1996.

NASA, Advances in sterilization and decontamination, *NASA Spec. Publ., SP-5105*, 1978.

NASA, Mars Sample Handling and Requirements Panel (MSHARP) Final Report, *NASA Tech. Memo., TM-1999 – 209145*, 1999.

Nyquist, L. E., B. M. Bansal, H. Wiesmann, and C.-Y. Shih, Neodymium, strontium and chromium isotopic studies of the LEW86010 and Angra dos Reis meteorites and the chronology of the angrite parent body, *Meteoritics, 29*, 872-885, 1994.

Pederson, L. R., Chemical implications of heat and radiation damage to rock salt, in *Scientific Basis for Nuclear Waste Management*, edited by C. M. Jantzen, J. A. Stone, and R. C. Ewing, pp. 701-708, Mater. Res. Soc., Pittsburgh, Pa., 1985.

Ratner-Zohar, Y., A. Banin, and Y. Chen, Oven drying as a pretreatment for surface area determination of soils and clays, *Soil Sci. Soc. Am. J., 47*, 1056-1058, 1983.

Richmond, J. Y., and J. S. Walker, Gamma irradiation as a means of inactivating animal disease microorganisms, *Am. Assoc. Veterinary Lab. Diagnosticians Annu. Proc., 25th*, 433-440, 1982.

Roedder, E., Fluid Inclusions, *Rev. Mineral.*, vol. 12, 646 pp., Mineral. Soc. of Am., Washington, D. C., 1984.

Ruff, S. W., P. R. Christensen, P. W. Barbera, and D. L. Anderson, Quantitative thermal emission spectroscopy of minerals: A laboratory technique for measurement and calibration, *J. Geophys. Res., 102*, 14,899-14,913, 1997.

Shulman, J. H., and W. D. Compton, *Color Centers in Solids*, Macmillan, Indianapolis, Ind., 1962.

Simon, I., *Infrared Radiation*, D. Van Nostrand, Princeton, N. J., 1966.

Space Studies Board, *Mars Sample Return Issues and Recommendations*, Natl. Res. Counc., Washington, D. C., 1997.

Spitsyn, V. I., B. D. Balukova, I. M. Kasarove, and S. A. Kabakchi, Experimental evaluation of changes in properties of natural minerals under irradiation, in *Scientific Basis for Nuclear Waste Management III*, edited by J. G. Moore, pp. 429-433, Plenum, New York, 1981.

Spitsyn, V. I., B. D. Balukova, and M. K. Savushkina, Influence of irradiation with gamma quanta and beams of accelerated electrons on the sorption parameters of clay minerals of the montmorillonite group, in *Scientific Basis for Nuclear Waste Management IV*, edited by S. V. Topp, pp. 703-707, Elsevier Sci., New York, 1982.

Squyres, S. W., et al., The Athena Mars rover science payload, *Lunar. Planet. Sci. [CD-ROM], XXIX*, abstract 1101, 1998.

Stewart, D. B., G. W. Walker, T. L. Wright, and J. J. Fahey, Physical properties of calcic labradorite from Lake County, Oregon, *Am. Mineral., 51*, 177-197, 1966.

Van Olphen, H., and J. J. Fripiat, *Data Handbook for Clay Minerals and Other Non-Metallic Materials*, Pergamon, Tarrytown, N. Y., 1979.

Vityk, M. O., and R. J. Bodnar, Statistical microthermometry of synthetic fluid inclusions in quartz during decompression, *Contrib. Mineral. Petrol., 132*(2), 149-162, 1998.

Weidner, V. R., and J. J. Hsia, Reflection properties of pressed polytetrafluoroethylene powder, *J. Opt. Soc. Am., 71*, 856-861, 1981.

Wopenka B., B. L. Jolliff, E. Zinner, and D. T. Kremser, Trace-element zoning and incipient metamictization in a lunar zircon: Application of three different microprobe techniques, *Am. Mineral., 81*, 902–912, 1996.

F. G. Albert, and J. Combie, Montana Biotech Corporation, Belgrade, MT 59714. (mtbiotech@montana.net).

C. C. Allen, Lockheed Martin Space Operations, 2400 NASA Road 1, Houston, TX 77058. (carlton.c.allen1@jsc.nasa.gov)

A. Banin, I. Kan, and Y. Yablekovitch, Department of Soil and Water Sciences, Hebrew University, Rehovot, Israel. (banin@agri.huji.ac.il)

R. J. Bodnar, Department of Geological Sciences, Virginia Polytechnic Institute and State University, Blacksburg, VA 24061. (bubbles@vt.edu)

V. E. Hamilton, Department of Geology, Arizona State University, Box 871404, Tempe, AZ 85287. (hamilton@east.la.asu.edu)

B. L. Jolliff, K. Kuebler, and A. Wang, Department of Earth and Planetary Sciences, Campus Box 1169, One Brookings Drive, Washington University, St. Louis, MO 63130. (blj@levee.wustl.edu)

D. J. Lindstrom, NASA Johnson Space Center, 2101 NASA Road 1, Houston, TX 77058. (david.j.lindstrom1@jsc.nasa.gov)

P. A. Morris, Department of Natural Science, University of Houston -- Downtown, 1 Main Street, Houston, TX 77002. (smithp@dt.uh.edu)

R. V. Morris, NASA Johnson Space Center, 2101 NASA Road 1, Houston, TX 77058. (richard.v.morris1@jsc.nasa.gov)

R. W. Murray, Department of Earth Sciences, Boston University, 685 Commonwealth Avenue, Boston, MA 02215. (rickm@bu.edu)

L. E. Nyquist, NASA Johnson Space Center, 2101 NASA Road 1, Houston, TX 77058. (laurence.e.nyquist1@jsc.nasa.gov)

P. D. Simpson, Centers for Disease Control and Prevention, Atlanta, GA 30333. (pds1@cdc.gov)

A. Steele, University of Portsmouth, Portsmouth, England P01 2DT. (andrew.steele@easynet.co.uk)

S. J. Symes, NASA Johnson Space Center, 2101 NASA Road 1, Houston, TX 77058. (steven.j.symes1@jsc.nasa.gov)

(Received April 8, 1999; revised August 2, 1999;
accepted August 5, 1999.)